Synthesis of Molybdenum Disulfide for the Removal of Progesterone from Water

Bessai, Sam
九州大学大学院総合理工学府総合理工学専攻地球環境理工学メジャー

KYUSHU UNIVERSITY

INTERDISCIPLINARY GRADUATE SCHOOL OF ENGINEERING SCIENCES

EARTH SYSTEM SCIENCE & TECHNOLOGY

WATER & ENVIRONMENTAL ENGINEERING LABORATORY

Synthesis of Molybdenum Disulfide for the Removal of Progesterone from Water

MSc Thesis

by

SAM BESSAI

BSc Env Eng (Guelph)

Academic Supervisor

Assoc. Prof. Osama Eljamal

July 2024

Abstract

Clean water is a fundamental human right. Water sources contaminated with hormone-disrupting chemicals like progesterone present a potential risk to the environment and human health. Molybdenum disulfide (MoS_2) nanoparticles are investigated in this work as a promising water treatment technology to help remediate these issues. The results of this study indicate that progesterone was effectively removed from water using MoS_2 nanoparticles, with removal efficiencies as high as 98% within an hour of contact. The effects of environmental conditions like temperature, pH, dosage and initial progesterone concentration on the removal efficiency were investigated. Based on the findings, the optimal removal efficiency was obtained at an operating temperature of 25°C, a neutral pH (7), a MoS_2 dosage of 20 mg L^{-1} and an initial progesterone concentration of 20 mg L^{-1}. Notably, MoS_2 nanoparticles maintained high performance across a broad range of tested conditions. Analysis of the removal mechanisms indicated that Van der Waals forces, hydrogen bonds and electrostatic interactions are some of the synergistic adsorption mechanisms that are involved in the removal process. Additionally, it was determined that MoS_2 nanoparticles are an affordable choice for water treatment since they can be manufactured and reused many times without experiencing a major reduction in performance. While MoS_2 nanoparticles show great promise, further research is needed to fully realize their potential. Important future research includes investigating large-scale production techniques, creating effective protocols for regeneration, and conducting pilot-scale studies. MoS_2 nanoparticles are highly effective at treating progesterone-contaminated water and support larger initiatives to improve water quality.

Acknowledgements

In the name of Allah, to whom belongs all praise and worship. I would like to express my greatest debt to my supervisor, Assoc. Professor Osama Eljamal, who has firmly supported me over the past two years. It has been a privilege to work under his guidance and benefit from his extensive knowledge and experience. His unwavering mentorship and encouragement have been paramount to my academic and professional journey.

My sincere thanks to all my colleagues in the Water and Environmental Engineering Laboratory (WEEL), the administrative staff in the Department of Earth Systems Science and Technology (ESST) and Student Affairs. I am humbled by the kindness and support you have shown me.

I owe a debt of gratitude to my father for his unwavering support and modeling of dedication, skill and determination. I would be proud to be a tenth of the man he is. I must thank my mother for offering me support and advice without which I could never have completed this undertaking. Her encouragement and prayers have been a constant source of strength.

I could never adequately thank all those who have made this thesis possible. Enumerating the names and detailing the contributions of everyone who aided me in this endeavor would not do justice in a few words.

Table of Contents

List of Tables

List of Figures

Chapter 1

Introduction

1.1 Background

Water is essential to life on Earth, and it is indispensable for the survival of all living organisms. Covering approximately 71% of the Earth's surface, water is one of the most abundant resources on our planet [1]. However, despite its apparent abundance, only 3% is readily available for human consumption in the form of freshwater from lakes, reservoirs, and rivers. Moreover, less than 1% is accessible to humans since most of the planet's freshwater is locked in glaciers or beneath the Earth's surface [2]. Water is a fundamental nutrient for the healthy function of every cell in the body. It performs operations like regulating internal body temperature, metabolizing and transporting macronutrients in the bloodstream, assisting in waste removal, acting as a protective barrier for the brain and spinal cord, lubricating the joints and performs many other vital functions [3].

The limited availability of this invaluable resource poses significant challenges, especially as the world's population continues to rise and industrialization proliferates [4][5]. Ensuring that all living organisms have access to clean and safe drinking water is a top priority.

1.2 Water Pollution

1.2.1 Definition

Water pollution refers to the presence of an unwanted substance that renders the water impure or compromise its quality and safety. Although the terms "pollutants" and "contaminants" are often used interchangeably, a pollutant specifically refers to a substance that, when introduced into the environment, causes harm or stress to life and ecosystems. Pollutants are typically associated with anthropogenic activity. In contrast, contaminants are any substances, whether naturally occurring or otherwise, that are present in an environment where they do not belong or are found at higher concentrations than normal [6].

1.2.2 Types of water pollution

Pollutants come in many different shapes and sizes and can affect our rivers, lakes, aquifers, oceans, and all other bodies of water [7]. These pollutants many include biological agents (pathogens, algae), physical factors (heat, radiation), chemical substances (organic and inorganic matter) or radioactive materials (uranium, chromium) [8][9][10]. Water is considered a universal solvent, meaning it can dissolve a plethora of substances. This property is due to the polar nature of water

molecules, which allows them to interact with various substances, evenly integrating them throughout the solution, ultimately deteriorating water quality and making it toxic to humans and the environment [11].

1.2.3 Sources of water pollution

Pollution can enter our water systems from various sources, each presenting distinct challenges. These sources are categorized into point and nonpoint sources. Point source pollution originates from a single, identifiable discharge source, making it easier to identify, monitor, and regulate [12][13]. Primary sources of water pollution include industrial discharge, power generation, and mining activities, agricultural and urban runoff, sewage and wastewater, illegal dumping, and the infiltration of chemicals from landfills and contaminated sites [14]. Point source pollution is typically managed by regulatory agencies like the Environmental Protection Agency (EPA). Conversely, nonpoint source pollution originates from diffuse sources, lacking a single point of origin or outlet. These sources are often widespread, making them difficult to contain, manage and regulate [15][16]. Pesticides and fertilizers carried by agricultural runoff are common examples of nonpoint source pollution. Additionally, sedimentation from construction sites, acid rain, and urban runoff contribute to nonpoint source pollution. These diffuse sources infiltrate water bodies introducing, introducing a variety of different that spread widely, complicating regulation and control [16].

1.3 Environmental Impact and Management

1.3.1 Pharmaceuticals and Personal Care Products (PPCPs)

Pharmaceuticals and personal care products (PPCPs) encompass a wide range of chemicals, including prescription and over-the-counter drugs, as well as non-medicinal consumer products that like fragrances [17]. PPCPs are used by consumers for personal health, cosmetics, and household cleaners, or by agribusinesses to enhance livestock [18][19]. PPCPs can infiltrate the environment through various routes, including human and animal excretion, improper disposal, urban and agricultural runoff, and industrial discharge. These pollutants originate from both point and nonpoint sources and are known for their persistence in the environment. PPCPs often pass through water treatment plants untreated and are subsequently released into the surrounding environment [20].

1.3.2 Endocrine Disrupting Chemical (EDC)

Endocrine Disrupting Chemicals (EDCs) are substances that can interfere with the body's endocrine system. The endocrine system releases hormones into the bloodstream via glands, regulating a various biological processes such as growth, metabolism, and reproduction [21]. Disruption of this system can lead to serious health issues, and EDCs are surprisingly found in everyday products, including cosmetics, food packaging, detergents, furniture, and textiles [22][23]. EDCs enter the environment through several different pathways, originating from both point and nonpoint sources. These chemicals have been linked to neurological, immune, metabolic, and reproductive health issues [22].

1.3.3 Progesterone

Progesterone (PGS) is a steroid hormone produced in the human body that is responsible for regulating numerous processes. It is composed of three cyclohexane rings and one cyclopentane ring fused together, as depicted in **Figure 1**. It also contains a ketone group, a hydroxyl group, methyl groups, and a double bond.

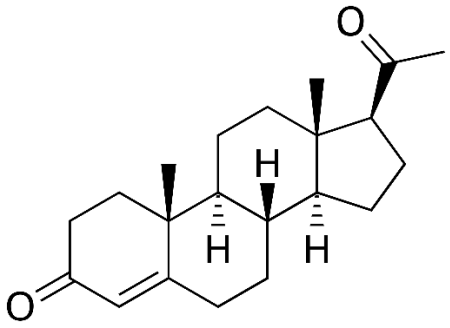

Figure 1: Chemical structure of progesterone ($C_{21}H_{30}O_2$)

In the female body, PGS is produced in the ovaries, adrenal gland, and placenta, where it is regulates menstrual cycles, supports pregnancy, promotes breast development, and modulates the immune system [24][25]. Although PGS is often considered the "female hormone", it is also produced in males through the testes and adrenal glands. While it does not play a significant role in men as in women, PGS is involved in the biosynthesis of testosterone, regulation of the nervous system, mood influence, spermatogenesis, and maintenance of bone health [26][27]. Once

produced, PGS is transported to the nervous system; however, it is also synthesized within the nervous system throughout a person's lifetime, earning it the designation of a neurosteroid [28].

The birth control pill, or the oral contraceptive pill, is the most prescribed drug for women, with approximately 25% of American women between the age of 15-44 reporting its use [29]. Over 150 million women worldwide currently use birth control pills, and according to the World Health Organization (WHO), this number is projected to skyrocket to approximately 800 million by 2030 [30][31]. Correspondingly, the market for oral contraceptives is expected to grow by an additional 13%, reaching around $2.1 billion by that year. Synthetic PGS is the primary ingredient for oral contraceptives, typically formulated either as a combination pill with PGS and estrogen, or as a PGS-only pill. It is also frequently prescribed for hormone replacement therapy, menstrual disorders, preterm birth prevention, and regulating menopause symptoms [32][33].

1.3.4 Environmental Occurrence and potential entry pathways

Due to the widespread use of PGS, it is increasingly detected in the environment at concentrations ranging from μg L^{-1} to ng L^{-1} [34]. Both synthetic and natural PGS enter the environment through various anthropogenic pathways as illustrated in **Figure 2**, which depicts the pathways and environmental impacts of PGS arising from human and industrial sources. A significant portion of PGS consumed by humans enters the bloodstream, then undergoes metabolism in the liver, resulting in various PGS derivatives. These forms are then excreted either unmodified or as metabolites through urine and feces, eventually makes their way to the wastewater treatment plants (WWTPs). Conventional WWTPs are often incapable of thoroughly removing steroid hormones, leading to measurable concentrations of effluent PGS being discharged into both aquatic and non-aquatic environments, such as lakes, rivers, and soil [34]. Additionally, certain agricultural practices and livestock farming contribute to the leaching of PGS into the soil and water bodies through surface runoff and infiltration [35]. Improper disposal of waste from the pharmaceutical manufacturing industry is another pathway through which high levels of PGS enter our environment. Once present in nature, PGS can cycle between aquatic and non-aquatic environments, posing potential risks to many ecosystems. Moreover, household products like creams and lotions introduce PGS into the aquatic environment via domestic wastewater [36]. Several studies have reported high levels of PGS in regional water bodies, with concentrations in the ng L^{-1} range, including concentrations as high as 16,689 ng L^{-1} in the Kalansanan River in

Malaysia [37][38][39][40][41]. These findings highlight the prevalence of PGS in the environment and the need for improved wastewater management and treatment strategies to mitigate its environmental impacts.

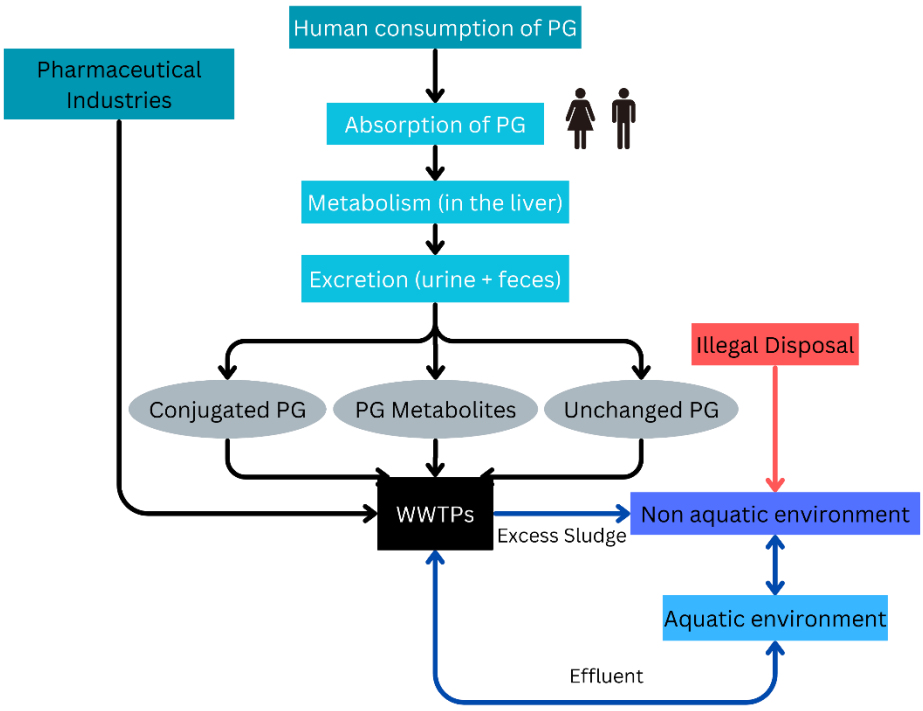

Figure 2: Sources and pathways for the occurrence of progestins in the environment. Adapted from M.J. Rocha and E. Rocha, "Synthetic Progestins in Waste and Surface Waters: Concentrations Impacts and Ecological Risk", *Toxics,* Vol. 10, no. 4, p. 163, 2022. [Online]. Available: **https://doi.org/10.3390/toxics10040163**. Licensed under CC BY 4.0.

1.3.5 Potential threats and ecosystem

PGS poses a significant threat to humans and ecosystems and is found in various environmental sources like water bodies, and foods [42][37]. The WHO has identified PGS as a Contaminants of Emerging Concern (CECs).These are chemicals and substances that pose a threat to human health and aquatic life, and are being detected at increasing levels in the environment [17]. These CECs are not fully understood yet and are a major focus of ongoing research. PGS happens to fall under the category of PPCPs and EDCs from the list of CECs due to its extensive application in the pharmaceutical industry and its potential interference with the endocrine system. PGS remains

biologically active long after excretion, posing a significant treat to human health and aquatic ecosystems.

Studies have shown that exposure to high levels of PGS reduces embryotic development, causing abnormalities and increasing mortality in some species [43][44][45]. Notably, exposure to PGS have been linked to significant disruption in rainbow trout, leading to the development of eggs within the testes of male fish and intersex conditions where fish exhibit both male and female characteristics [46][47]. The hormonal imbalances caused by PGS result in physiological alterations and reproductive issues, which can create a cascading effect throughout the food chain, leading to a systematic imbalance in aquatic ecosystems. Furthermore, PGS is known to bioaccumulate in aquatic organisms, leading to higher and higher concentrations up the food chain, making larger organisms more susceptible to physical and developmental irregularities [48].

The consequences of PGS contamination extend beyond aquatic species. PGS is also known to disrupt soil microbes necessary for nutrient cycling and plant growth, impacting soil health and fertility [49]. This disturbance to the terrestrial ecosystem can cause adversely affect food sources and indirectly expose humans through consumption [50]. The presence of PGS thus poses multiple threats to human health and the ecosystem, although the full extent of its damage remains unknown [51].

1.3.6 Treatment of Progesterone Pollution

To mitigate the detrimental effects of PGS pollution on ecosystems, it is crucial to establish effective treatment methods. Prevention is the best approach, starting with the developing sustainable disposal procedures should be the initial course of action. For PGS that is excreted by the body, utilizing advanced filtration and degradation technologies and optimizing wastewater treatment facilities are effective treatment practices. One effective method for removing PGS from wastewater is the use of activated carbon, which effectively adsorbs PGS onto its surface [52]. However, this technology has drawbacks, including high cost, regeneration and disposal issues, limited adsorption capacity, and environmental impact [53][54].

Another method for removing PGS from water is advanced oxidation processes (AOPs). AOPs, such as ozonation, UV/H_2O_2, and Fenton reactions, degrade PGS into less harmful compounds using highly reactive species [55][56]. Despite their effectiveness, AOPs have limitations, including high energy costs, potential hazardous byproduct formation, and the need for highly

specialized equipment for handling reactive species [57][55]. Technologies such as nanofiltration and reverse osmosis are also effective but are costly and require regular maintenance [58][59]. Additionally, biological treatment methods have also shown promise in managing PGS pollution in water sources. Microbes in bioreactors and constructed wetlands can break down PGS into harmless compounds, offering a sustainable, cost-effective treatment option [60]. However, the effectiveness of this approach is highly sensitive to microbial activity, treatment time, and environmental conditions such as temperature, pH, oxygen, and nutrient availability [61][62].

While advanced methods for PGS removal exist, their widespread use is limited by cost and complexity [51]. Sustainable bio-treatment methods are appealing but depend heavily on specific conditions. To address this issue, a combination of responsible disposal, and the development of new, more efficient treatment solutions is required. This comprehensive approach can effectively manage PGS and protect the environment.

1.4 Molybdenum Disulfide (MoS_2)

1.4.1 Background

Molybdenum disulfide (MoS_2) has recently garnered significant interest due to its unique properties and wide range of applications. MoS_2 is a layered transition metal dichalcogenide (TMD) consisting of a transition metal atom (molybdenum) between chalcogen atoms (sulfur), held together by weak Van der Waals forces that allow it to exfoliate into thin monolayer sheets [63]. Several methods exist for synthesizing molybdenum disulfide, each yielding specific properties. MoS_2 was first used as a dry lubricant in industrial applications because of its low-friction coefficient and high temperature stability [64]. It has since found applications in advanced technologies such as catalysis and photocatalysis, transistors and sensors, energy storage, and semiconductors [65][66][67]. MoS_2 is particularly valued in electronic applications due to its physical, chemical, and electronic properties.

In catalysis, MoS_2 has exhibited significant potential, particularly in the hydrogen evolution reaction (HER), due to its numerous active sites for catalytic reactions [68]. Its catalytic performance can be further improved with the use of dopants and the creation of defects [69]. Recently, MoS_2 has gained popularity in environmental applications, especially in water treatment. MoS_2 offers a high surface area, superior chemical stability, and a strong affinity for adsorbing and

degrading contaminants like heavy metals and organic pollutants in water [70][71][72]. The use of MoS_2 in environmental applications is certainly a promising area of research.

1.4.2 Removal mechanism of organic pollutants by MoS_2 nanoparticles

Several removal mechanisms are involved in the treatment of organic pollutants using MoS_2, with adsorption being the most dominant. Molybdenum disulfide has a high surface area, providing numerous active sites for water contaminants to adsorb [72]. Depending on the contaminant and conditions, this adsorption involves various interactions, including Van der Waals forces, hydrophobic interactions, or $\pi - \pi$ interactions [73]. Another removal mechanism is photocatalysis, where MoS_2 effectively degrades organic pollutants by generating electron-hole pairs due to its direct bandgap of 1.8 eV. These holes emerge on the surface of MoS_2, forming reactive oxygen species (ROS) like hydroxyl radicals ($\cdot OH$) and superoxide anions (O_2·-). These ROS then break down the organic compounds into less harmful molecules, eventually mineralizing into water and carbon dioxide [74].

Catalytic degradation is another mechanism, particularly in Fenton-like reaction and other degradation processes catalyzed by MoS_2. MoS_2 facilitates the breakdown of hydrogen peroxide (H_2O_2), and transition metal ions activate H_2O_2, producing strong hydroxyl radicals that decompose organic contaminants into simpler, less hazardous compounds [75]. In conclusion, multiple removal mechanisms can be involved in treating organic pollutants with MoS_2, and synergistic effect may occur when these mechanisms work together. Adsorption/desorption studies, isotherm modeling, and control experiments can help identify the specific removal mechanisms at play [76].

1.4.3 Defects and improvement techniques of MoS_2

Introducing defects in MoS_2 can significantly enhance its performance, tailoring the material to specific applications. The most common defect is the introduction of sulfur vacancies, which improve MoS_2's electronic and catalytic properties [77]. Molybdenum vacancies may also affect these properties, though their impact is less pronounced [78]. Additionally, doping with other elements has been shown to alter MoS_2's properties, especially in industrial, optical, and electrical applications [79][69][80]. During the synthesis, attaching functional molecules or coating MoS_2 with polymers has also been shown to enhance its catalytic properties and environmental degradation performance, respectively [81][82]. Furthermore, exfoliation techniques can be used

to produce monolayer or few-layer MoS_2, improving its optical and electrical properties. Common methods include liquid-phase exfoliation, mechanical exfoliation, and chemical exfoliation [83][84]. These are just a few of many ways that have been explored to optimize MoS_2 nanoparticles for specific applications.

1.4.4 Previous application of MoS_2 for the removal of progesterone

At the time of this study, no research had been conducted on the removal of PGS using MoS_2. This gap in the literature illustrates the necessity and originality of this research. While there have been studies regarding the removal of heavy metals in water using MoS_2 showing excellent results, scant research has been conducted in relation to organic pollutants and steroid hormone removal [85]. Some studies have successfully used MoS_2 to treat CECs from water, such as organic dyes and the antibiotic ciprofloxacin [86]. The unique properties of MoS_2 suggest it could be effective in removing organic pollutants, including hormones. Its high surface area, numeration activation sites and physiochemical interactions, along with its potential for photocatalytic degradation, make MoS_2 a strong candidate for PGS removal.

1.4.5 Benefits of MoS_2 over NZVI

In the early efforts to remove PGS from water, nanoscale zero valent iron (NZVI) was extensively studied. Numerous batch experiments were conducted using various forms of NZVI, including bare NZVI, magnesium-coated NZVI, NZVI-oxalate nanocomposite, NZVI-EDT nanocomposites as summarized in Supplementary Table 1. However, none of these methods showed significant promise. The primary disadvantage of using NZVI is its rapid oxidation in the presence of PGS, possibly due to a chelating effect that accelerates NZVI oxidation [87]. After filtering the NZVI, the samples would quickly turn yellow, interfering with the UV-spectrophotometry analysis.

Various solutions to prevent this rapid oxidation were investigated, such as adding H_2O_2 and ascorbic acid as reducing agents to donate electrons in the redox reaction. While theoretically promising, these approaches proved insufficient in practice, leading to further issues such as PGS precipitation. These findings are also summarized in Supplementary Table 1. Diluting the samples and modifying the analytical procedure were similarly ineffective.

Long-term experiments using NZVI nanoparticles demonstrated better results, as can be seen in Supplementary Table 2 and Supplementary Table 3. The highest removal efficiency achieved was

between 24-36 hours with a measured removal efficiency of over 70%. However, this considerable contact, combined with the instability of PGS under various conditions, as illustrated in Figure 4, suggests that the high removal efficiency may be due to the physical and chemical breakdown of the PGS molecule and/or its instability in long-term storage, rather than the direct interaction with NZVI nanoparticles. These experiments indicate that NZVI is incompatible with effectively removing PGS from water, primarily due to undesired oxidation. Further modification of NZVI may yield more promising results.

1.5 Research aim and objectives

The purpose of this study is to investigate the effectiveness of MoS_2 nanoparticles in removing PGS from water. This research aims to fill the gap in the current literature by exploring a novel water remediation technique, evaluating its performance, and suggesting practical applications for MoS_2 in treating water contaminated with steroid hormones like PGS. This study seeks to contribute to the development of innovative water treatment technologies. The detailed objectives are as follows:

- Design an experimental procedure.
- Synthesize MoS_2 nanoparticles using a simple hydrothermal method.
- Characterize MoS_2 nanoparticles to reveal their physicochemical properties and verify their structure.
- Evaluate the performance of MoS_2 nanoparticles in treating PGS-contaminated water under varying conditions of pH, temperature, MoS_2 dosage, and initial PGS concentration.
- Optimize the conditions to maximize PGS removal efficiency.
- perform desorption experiments to determine the removal mechanism of PGS by MoS_2 nanoparticles.
- Analyze the experimental results using kinetic modeling to understand the interaction between PGS and MoS_2 nanoparticles.
- Assess the economic feasibility of using MoS_2 at an industrial scale and propose potential future investigations.

By successfully achieving these objectives, this study will provide a comprehensive understanding of the effectiveness of MoS_2 nanoparticles in treating PGS-contaminated water.

1.6 Thesis outline

The master's thesis framework comprises four chapters:

Chapter 1: This chapter provides a background on water pollution by PPCPs and EDCs, with a focus on progesterone. It also explores treatment approaches, discusses MoS_2's current use in treating contaminated water, and identifies gaps in existing research. Furthermore, it examines the occurrence, fate, health risks, and ecotoxicity of PGS. The aims and objectives are discussed near the end of the chapter, along with the thesis outline.

Chapter 2: This chapter creates a catalogue of the chemicals used, details the step-by-procedure for synthesizing MoS_2, and describes the characterization methods employed. Additionally, the analytical tools, modeling techniques, and batch experiments are discussed.

Chapter 3: This chapter presents a comprehensive investigation of MoS_2 nanoparticles for the removal of PGS, including treatment techniques, removal mechanisms, and performance evaluation under various conditions. This chapter also delve into economic feasibility and the potential impact of water matrix components on the removal process.

Chapter 4: This chapter highlights significant findings and conclusions and offers suggestions for future research.

Chapter 2

Materials and Methods

2.1 Chemicals and materials

Table 1: List of chemicals used for this study.

Chemical Name	Specification	Company	Application
Progesterone	$C_{12}H_{30}O_2$, MW=314.46 g mol^{-1}, Purity > 98%	TCI, Japan	Preparation of PGS stock solution
Ammonium Molybdate Tetrahydrate	$(NH_4)_6MO_7O_{24} \cdot 4H_2O$, MW=1236.03 g mol^{-1}, Purity = 99%	FUJIFILM Wako Pure Chemical Corporation, Japan	MoS_2 nanoparticle synthesis
Thiourea	CH_4N_2S, MW= 76.14 g mol^{-1}, Purity = 99%	Sigma-Aldrich, USA	MoS_2 nanoparticle synthesis
Ethanol	C_2H_5OH, MW = 46.07 g mol^{-1}, Purity = 99.5%	FUJIFILM Wako Pure Chemical Corporation, Japan	Dissolving PGS into the stock solution
Sodium hydroxide	NaOH, MW= 40.00 g mol^{-1}, Purity = 97%	JENSEI, Japan	pH adjustment and desorption
Hydrochloric acid	HCl, MW = 36.46 g mol^{-1}, Standard content = 35 ~ 37%	FUJIFILM Wako Pure Chemical Corporation, Japan	pH adjustment

2.2 Synthesis of Molybdenum Disulfide (MoS_2)

Molybdenum disulfide was synthesized following the hydrothermal method described by Zhou et al. [88] and summarized in the following equation:

$$(\mathbf{NH_4})_6\mathbf{MO_7O_{24}} \cdot \mathbf{4H_2O} + \mathbf{21C}\boldsymbol{CH_4N_2S} \rightarrow \mathbf{7}\boldsymbol{MoS_2} + \mathbf{21}\boldsymbol{CO_2} + \mathbf{39}\boldsymbol{NH_3} + \mathbf{20}\boldsymbol{H_2O} \quad \textbf{(1)}$$

In this method, 0.6g of ammonium molybdate tetrahydrate ($(NH_4)_6MO_7O_{24} \cdot 4H_2O$) and 1.2g of thiourea ($CH_4N_2S$) were dissolved and added to 70 mL of ultrapure deionized (UPDI) water while stirring vigorously. The mixture was then transferred to a 100 mL Teflon-lined stainless-steel autoclave and kept at 200°C for 20 hours. The autoclave was subsequently removed and set aside to cool to ambient temperature. Upon cooling, the mixture was placed into a centrifuge, and the precipitate was collected and washed three times with anhydrous ethanol and UPDI water. The precipitate was placed in a vacuum dryer at 70°C overnight. The final step involved heating the powder from 200° at an increasing rate of 10°C min^{-1} for 2 hours to introduce sulfur defects and oxygen incorporation, as expounded by Zhou et al. [88]. The crystalline structure and chemical composition of MoS_2 were evaluated using X-ray diffraction analysis (XRD, Smartlab, Rigaku, Japan).

2.3 Characterization of nanomaterials

The physicochemical properties of MoS_2 were characterized using advanced analytical instruments, including X-ray diffraction (XRD), Brunauer-Emmett-Teller (BET), and scanning electron microscopy (SEM). The following subsections detail each of these methods.

2.3.1 X-ray Diffraction (XRD)

X-ray diffraction (XRD) analysis is an advanced non-destructive characterization tool that directs X-rays at a crystalline sample and measures the angle and intensity of the diffracted beams. These diffracted beams help determine the spacing between the crystalline planes and provide information on the material's physicochemical structure [89][90]. The relationship between the incident angle of the scattered beams and the material's lattice planes is described by Bragg's Law:

$$\boldsymbol{n\lambda = 2dsin\theta} \quad \textbf{(2)}$$

Where n is the order of reflection, λ is the wavelength of the incident ray, d is the spacing between the crystalline planes, and θ is the incident angle [91]. The crystallographic structure, chemical

composition, and physical properties of MoS_2 were analyzed using XRD both before and after treating PGS. This analysis was performed using the D8 Advance (Bruker, Germany) for the clean MoS_2 sample then the TTR Rigaku diffractometer (Rigaku, Tokyo, Japan) was used for spent sample after treating PGS. The devices used Cu k_α radiation to produce X-rays with a wavelength of 1.5418 Å and a power output of 50 kV and 300 mA. Furthermore, the scanning angle was configured to a range between 0° and 90° at a scanning rate of 2° per minute.

2.3.2 Brunauer-Emmett Teller (BET)

Brunauer-Emmett-Teller specific surface area (SSA_{BET}) analysis measures the area per unit mass of a nanomaterial using gas adsorption techniques involving argon, krypton, or nitrogen [92]. In this study, the specific surface area and nitrogen adsorption-desorption isotherms for MoS_2 nanoparticles were determined at 77.15 K using a 3Flex surface characterization analyzer (Micromeritics Instrument, USA). Prior to analysis, the MoS_2 was heated and degassed at 623.15 K for two hours under a continuous flow of nitrogen gas to ensure the complete removal of any contaminants.

2.3.3 Scanning Electron Microscopy (SEM)

Scanning electron microscopy (SEM) collects data on the surface topography of nanomaterials by using a focused electron beam to scan the surface [93]. Although transmission electron microscopy (TEM) provides higher-resolution images compared to SEM, TEM analysis and sample preparation are more complex and time-consuming [94]. SEM images of the samples were captured using a JSM-IT700HR microscope (JEOL Ltd., Japan) at an operational voltage of 15 kV. This method allows for a detailed examination of changes in surface structure and morphology, providing important insights into the effects of PGS treatment on MoS_2 nanoparticles. Additionally, the SEM's relatively simple sample preparation and faster imaging capabilities make it the ideal method for surface characterization in this research.

2.4 Experimental procedures

2.4.1 Batch adsorption experiments

To investigate the effects of different parameters on the removal efficiency of PGS using MoS_2, the experimental design in Table 2 was carefully followed. 15 different modifications of MoS_2 were prepared using different synthesis methods and doping ratios. Initially, a preliminary investigation was conducted to determine which MoS_2 had the highest potential in removing PGS from water. Once this was completed and a single MoS_2 synthesis method was selected, comprehensive investigations on the selected MoS_2 were conducted. The MoS_2 dosage optimization experiment was executed by carefully measuring 4, 12, 20, 29, 40, and 60 mg of MoS_2 using a SHIMADZU ATX224 (SHIMADZU Co., Kyoto, Japan) analytical balance. These measured masses were then transferred into vials, followed by the addition of 10 mL of UPDI water. The water was sprayed onto the weighing dish to clean off any residue, and then it was decanted into the vials. The vials were ultrasonicated for 30 minutes to promote the dispersion of nanomaterials in the water.

Table 2: Batch experiment design for PGS removal using MoS_2.

Isolated variable	[PGS] (mg L^{-1})	MoS_2 dosage (mg L^{-1})	Initial pH	Temperature (°C)
Primary Conditions	20	100	7	25
Optimizing MoS_2 dosage	20	20-300	7	25
Optimizing initial pH	20	20	3 − 10	25
Optimizing reaction temperature	20	20	7	15−55
Optimizing PGS concentration	5−30	20	7	25

During ultrasonication, 200 mL Erlenmeyer flasks were set up for the batch experiment. Each flask was filled with 190 mL of the stock solution. After 30 minutes, the vials were removed from the

ultrasonic bath, and their contents were poured into the Erlenmeyer flasks containing the stock solution to make up 200 mL. The vials were then backwashed with the stock solution, as needed, to ensure the complete transfer of material. The flasks were positioned on a magnetic stirrer with a rubber stopper and agitated at 1000 rpm and 25 °C. After a designated contact period between MoS_2 and the contaminant, the stirrer was stopped for 5 minutes to allow some particulates to settle before sample extraction. Samples were extracted using a syringe, dispensed through a 0.45-µm filter (ADVANTEC Dimic, Japan), and collected in sample vials for analysis. The sampling procedure was repeated to obtain multiple samples for comprehensive analysis. This entire experimental procedure is illustrated schematically in Figure 3.

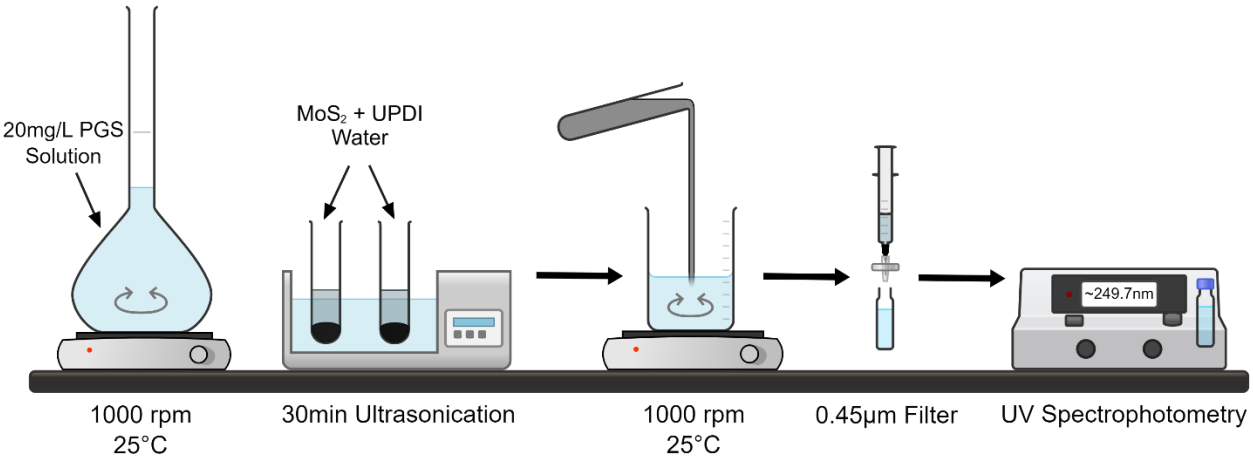

Figure 3: Schematic of batch experiment set up for the removal of PGS using MoS_2.

To investigate the effects of pH on removal efficiency, sodium hydroxide (NaOH) and hydrochloric acid (HCl) were used to modify the pH of 190 mL of PGS stock solution. The pH of the solutions was carefully modified to 3, 5, 7, and 10 using a Horiba LAQUA D-210P. Subsequently, 20 mg of MoS_2 was measured, ultrasonicated, and decanted into the 200 mL flasks. The pH was also recorded at the end of the experiment to ensure accuracy.

To assess the impact of temperature on the removal efficiency, the magnetic stirrer was preheated for 1 hour to ensure a consistent temperature throughout the 190 mL of stock solution before adding the 10 mL of ultrasonicated MoS_2-water mixture, starting the reaction. The temperatures tested were 15°C, 25°C, 35°C, 45°C, and 55°C. After preheating, 4 mg of MoS_2 was added to the preheated stock solution, and the mixture was agitated at 1000 rpm. Following the designated

contact period, samples were extracted and filtered as described above to analyze the effects of temperature on contaminant removal.

To assess the impact of initial contaminant concentration, a PGS stock solution with an initial concentration of 30 mg L^{-1} was prepared. This stock solution was then diluted to create a series of solutions with concentrations of 25, 20, 15, 10, and 5 mg L^{-1}. Subsequently, 10 mL of UPDI water containing 4 mg of ultrasonicated MoS_2 was added to 190 mL of each solution and agitated at 1000 rpm and 25°C. Following contact, samples were processed to determine how the initial PGS concentration impacted its removal.

2.4.2 Desorption and recycling experiment

To quantify the contribution of the adsorption mechanisms involved in the removal of PGS using MoS_2 nanoparticles, it is important to conduct a desorption experiment. After treating the PGS solution with MoS_2 nanoparticles, the nanoparticles were reclaimed using a vacuum filtration setup equipped with a 45-µm filter. The spent MoS_2 nanoparticles were placed in 0.2 L of 1 M NaOH solution while stirring at 1000 rpm and 25°C for 3 hours [95]. Recycling spent MoS_2 nanoparticles for multiple treatment cycles is important for enhancing sustainability and cost-effectiveness [96]. Evaluating the reusability of MoS_2 nanoparticles is crucial for environmental applications [97]. The regenerated MoS_2 nanoparticles from the desorption experiment were used for three treatment cycles, and the removal efficiencies were recorded after 1 hour of contact.

2.4.3 Longevity and storage experiment for progesterone solution

The longevity and storage conditions of PGS were carefully studied over a period of 3 days. Solutions containing 20 mg L^{-1} of PGS were subjected to various temperatures, agitation speeds, and light exposure to determine their effects on the concentration of PGS. The UV-spectroscopy absorbance values were recorded to monitor any changes. The results of this experiment are illustrated in Figure 4.

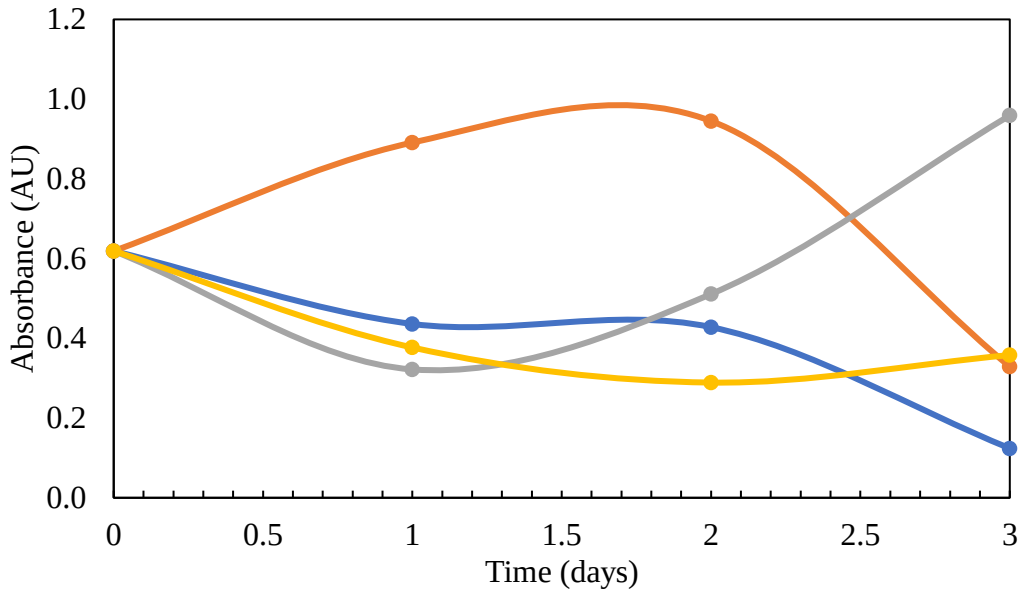

Figure 4: Stability of PGS solution over 3 days under various conditions of temperature, agitation and light exposure: 25°C, 1000 rpm, light (blue); 50°C, 1000 rpm, light (orange); 25°C, 1000 rpm, dark (gray); and 3°C, 0 rpm, dark (yellow).

Under the condition of 25°C with 1000 rpm agitation and light exposure, the absorbance values showed a steady decrease from 0.619 at the time of preparation to 0.124 on Day 3, indicating significant degradation of PGS under these conditions. By increasing the temperature to 50°C with similar agitation rate and light exposure, the absorbance values increased from 0.619 on Day 0 to a peak of 0.945 on Day 2 before decreasing to 0.329 on Day 3. This suggests an initial accumulation or concentration of some intermediates or breakdown products, followed by their degradation.

Next, the temperature was adjusted back to 25°C with 1000 rpm agitation and no light exposure (the sample was covered with aluminum foil). The absorbance initially decreased to 0.322 on Day 1 but increased to 0.959 by Day 3. This indicates possible photodegradation in light-protected conditions followed by reformation or stabilization of PGS or its byproducts.

Under the condition stored at 3°C with no agitation and no light exposure (stored in the fridge), the absorbance values showed minor fluctuations, decreasing from 0.619 on the day of preparation to 0.289 on Day 2, followed by a slight increase to 0.358 on Day 3. This indicates that lower

temperature and no light exposure helped maintain the stability of PGS with minimal degradation. Overall, the results suggest that light exposure and higher temperatures significantly accelerate the degradation of PGS. Furthermore, cooler, dark storage conditions help maintain its stability. The data also indicate that the preparation of the stock solution and its use should be conducted on the same day to prevent any degradation of PGS, which could cause unreliable results.

2.4.4 Sampling procedure valuation criteria

The experiment commenced by adding a specific amount of MoS_2 nanoparticles to the PGS solution in an Erlenmeyer flask. The flask was then placed on a magnetic stirrer (HSH-6D, AS ONE Corporation, Japan) set to 1000 rpm and a desired temperature. Samples were drawn from the flask at specific times depending on the experiment (ranging from 5 minutes to 2 hours) using a syringe (10 mL Luer lock, TERUMO, Japan). These samples were immediately filtered through a 0.45-micrometer filter (FILSTAR, Hawach Scientific, China) and stored for later analysis. The ability of MoS_2 to remove PGS was then measured by calculating removal efficiency [98]:

$$\boldsymbol{Removal\ efficiency}\ (\%) = \frac{(C_i - C_t)}{C_i} \times 100\% \qquad (3)$$

Where C_i represents the initial concentration of PGS (mg L^{-1}), and C_t represents the concentration at a specific time (min).

2.5 Analytical instruments

The concentration of the contaminant, PGS, in water samples was determined using UV-vis spectrophotometry (UV-1280, SHIMADZU, Japan). This method involves measuring the amount of light absorbed by the sample at a specific wavelength of 250 nm. To ensure accuracy, the instrument was first calibrated using standard solutions containing known concentrations of PGS (0.25, 0.5, 1, 5, 10, 15, and 20 mg L^{-1}). A calibration curve was generated by plotting the absorbance values recorded at 250 nm using the UV-1280 against their corresponding PGS concentrations, as depicted in Figure 5. This curve establishes a relationship between the measured absorbance and the actual PGS concentration in the unknown samples [99].

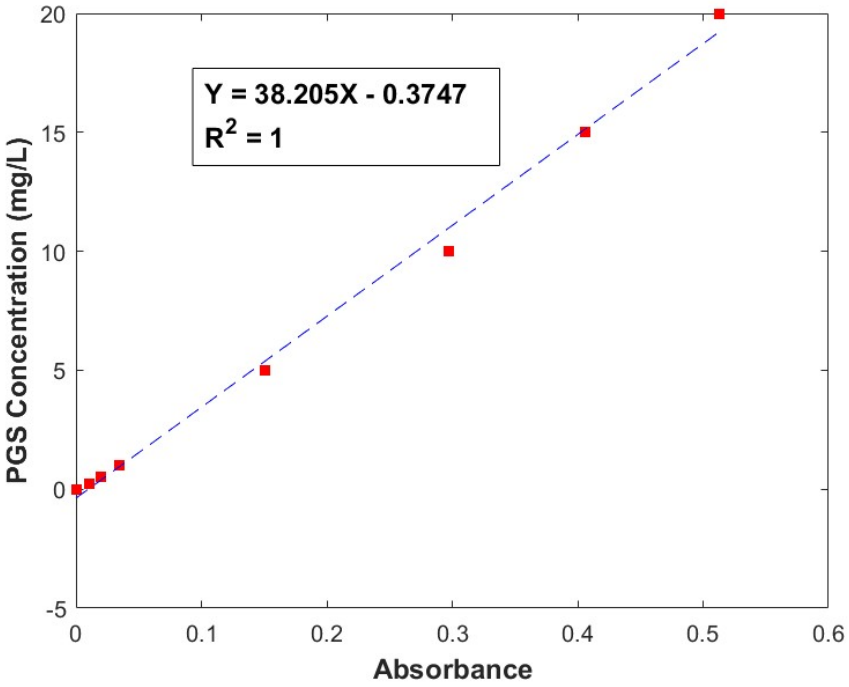

Figure 5: Calibration curve of PGS.

The calibration curve equation is denoted as:

$$Y = 38.205X - 0.3747 \qquad (4)$$

Where Y represents the PGS concentration (mg L^{-1}) and X represents the absorbance value measured by the UV-1280.

The calibration curve in Figure 5 demonstrates excellent linearity, indicated by a determination coefficient (R^2) of 1. This confirms the accuracy of the UV-vis spectrophotometry for PGS concentration measurements. For accurate measurement of PGS using MoS_2, samples were diluted with UPDI water prior to UV-1280 analysis. This dilution step was necessary to prevent excessive extraction of MoS_2 nanoparticles suspended in the water. Additionally, the mixing was stopped for 5 minutes to allow some of the suspended nanoparticles to settle at the bottom, further ensuring that minimal MoS_2 was extracted.

2.6 Modelling of progesterone adsorption

Kinetic modeling analysis was performed to understand the adsorption kinetics involved in the removal of PGS using MoS_2 nanoparticles. Furthermore, kinetic modeling elucidates the interaction mechanics by providing numerical results that distinguish between different adsorption types, such as physical adsorption and chemical adsorption [100].

2.6.1 Kinetic modeling

The kinetic analysis provides insight into the rate of PGS adsorption under various conditions and also estimates the speed at which adsorption takes place [101]. There are several models used to determine the kinetics of an adsorbent; however, the ones chosen for this study are Pseudo first-order, pseudo second-order, Elovich and intraparticle diffusion.

2.6.1.1 Pseudo-first order modeling

To describe the adsorption kinetics of PGS on the surface of MoS_2 nanoparticles, Lagergren proposed a pseudo-first order model with the following differential equation [102][103]:

$$\frac{dq_t}{dt} = k_1(q_e - q_t)$$

After some integration, the previous equation can be simplified with some boundary conditions as follows [104]:

$$\ln(q_e - q_t) = \ln(q_e) - k_1 t \quad (4)$$

2.6.1.2 Pseudo-second order modeling

Building on Lagergren's work, Blanchard et al. employed a pseudo-second-order model to characterize the removal of heavy metals by natural zeolites [105]. This model can be expressed through the following differential equation:

$$\frac{dq_t}{dt} = k_2(q_e - q_t)^2$$

After some integration with the assumed boundary conditions of time (t) = 0 and amount of absorbate absorbed (q) at time t = 0. The equation can be expressed as follows:

$$\frac{t}{q_t} = \frac{1}{k_2 q_e^{\,2}} + \frac{t}{q_e} \qquad (5)$$

2.6.1.3 Elovich model

In 1934, Roginsky and Zeldovich introduced the Elovich model to describe the chemosorption of carbon monoxide on the surface of manganese dioxide and is expressed by the following equation [106]:

$$\frac{dq_t}{dt} = \alpha \exp(-\beta q)$$

Integrating the equation takes the following form:

$$q_t = \frac{1}{\beta} \ln(1 + \alpha\beta t) \qquad (6)$$

2.6.1.4 Intraparticle diffusion model

Weber and Morris introduced the intraparticle diffusion model in 1962 to further understand the adsorption processes and derived the following equation [107]:

$$q_t = k_{intra} \cdot t^{0.5} + C \qquad (7)$$

These kinetics models provide an insight on the removal mechanism involved between PGS and MoS_2 nanoparticles. It also helps to reinforce the other investigations on the removal mechanism.

Chapter 3

Results and Discussion

3.1 Characterization of MoS_2

3.1.1 Scanning electron microscopy (SEM)

Scanning Electron Microscopy (SEM) analysis revealed key characteristics of the synthesized MoS_2 nanomaterial. Figure 6 displays an image of MoS_2 exhibiting an irregular, clustered morphology with particle sizes ranging from approximately 2 µm down to much smaller nanoparticles, indicating a heterogeneous size distribution. The nanoparticles appear to be aggregated to minimize the high surface energy [108]. Furthermore, a rough, uneven surface texture can be seen along with potential porosity between the small clusters, suggesting a high surface area for adsorption and catalytic reactions since they offer more active sites to interact with contaminants [109]. Overall, the SEM image of MoS_2 reveals a highly agglomerated structure with many surface irregularities and a heterogeneous size distribution. These characteristics typically indicate a high surface area with many activation sites, making these nanoparticles pertinent for water treatment applications [110]. The chosen synthesis method appears successful in producing high-quality nanomaterials with the desired structural features.

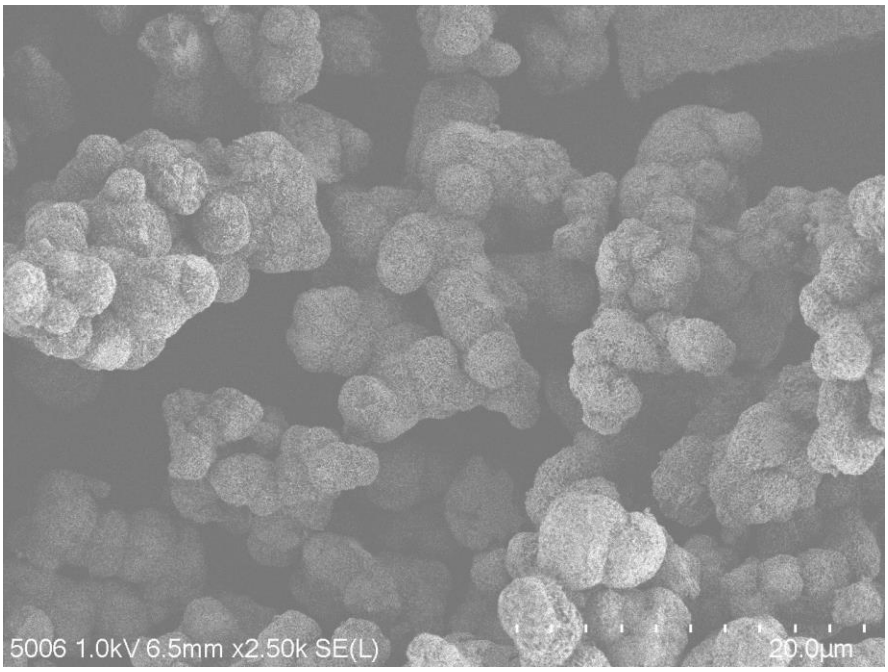

Figure 6: SEM image of MoS_2 nanoparticles.

3.1.2 X-ray diffraction analysis (XRD)

The crystalline structure and composition of the MoS_2 nanoparticles were examined using X-ray diffraction analysis (XRD, TTR, Rigaku Ltd., Japan). Figure 7 summarizes the XRD patterns for the MoS_2 nanoparticles. The XRD analysis in Figure 7 highlights several broad diffraction peaks corresponding to the structure of MoS_2. The most intense peak is observed at $2\theta = 14.4°$, which corresponds to the (002) plane. This demonstrates a large surface area with single layer stacking of crystalline MoS_2 along the c-axis, which is linked by weak Van der Waals bonding [111][112] [113]. Other prominent peaks appear at $2\theta = 32.7°$, 39.5°, and 58.3°, which can be attributed to the (100), (103), and (110) planes, respectively. These peaks confirm MoS_2 hexagonal structure, high crystallinity, nanoscale and purity [112][114]. These qualities are essential to a material's performance in many different applications including adsorption and catalysis.

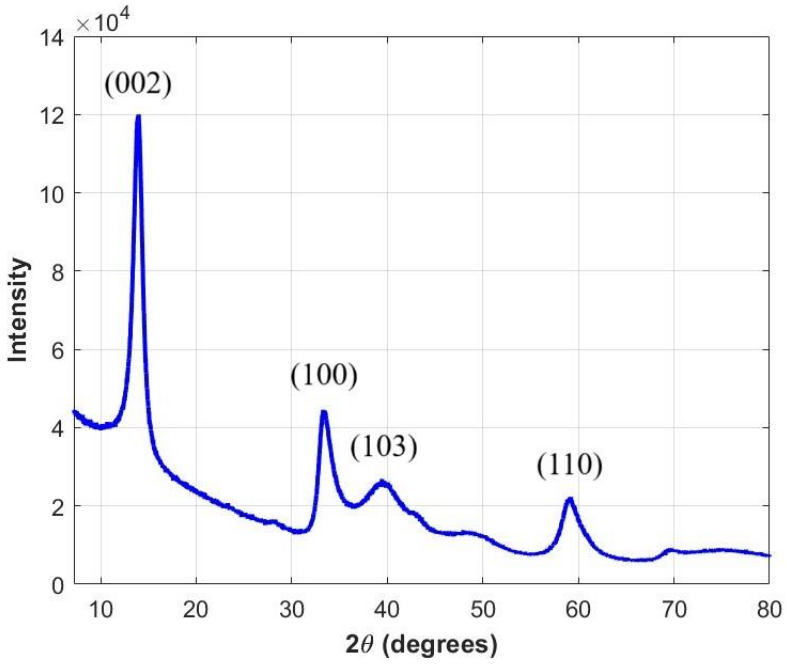

Figure 7: XRD analysis for MoS_2 nanoparticles.

3.1.3 Brunauer-Emmett-Teller Microscope (BET)

BET analysis of MoS_2 shows a moderate surface area of 0.241 m^2/g with mesopores using Barrett-Joyner-Halenda (BJH) analysis, suggesting some restrictions on total adsorption capacity. However, the existence of mesopores indicates the possibility of use in operations that involve the diffusion of larger molecules, such as catalysis and pollutant elimination. Moreover, the

nanoparticle demonstrates consistent and predictable adsorption-desorption characteristics, indicating its suitability for the removal of water contaminants in environmental applications.

3.2 Effects of MoS_2 dosage

The effects of MoS_2 dosage on the removal efficiency of PGS were evaluated using various dosages ranging from 20 mg L^{-1} to 300 mg L^{-1}. The optimal MoS_2 was determined based on its removal efficiency and minimal nanomaterial usage to ensure cost-effectiveness. The exact parameters for this analysis are summarized in Table 2. Figure 8 presents the results achieved from the MoS_2 dosage analysis after 1 hour and 2 hours of treatment time. Figure 8a shows the removal efficiency of PGS after 1 hour of treatment time at varying MoS_2 dosages. The highest removal efficiency was achieved with 20 mg L^{-1} of MoS_2, reaching a peak of 93.79%. However, as the dosage increased, the removal efficiency experienced slight drops: approximately 3.6% from 20 – 60 mg L^{-1}, 1.4% from 60 – 100 mg L^{-1}, and 4.1% from 100 – 145 mg L^{-1}. The lowest removal efficiency was observed after 1 hour of treatment at 85.49% using 145 mg L^{-1} of MoS_2 nanoparticles. Furthermore, after 145 mg L^{-1}, the removal efficiency began to rise steadily by a negligible amount, increasing by roughly 1% as the dosage increased. It is clear that beyond a certain dosage, any additional nanomaterial does not significantly enhance the removal efficiency.

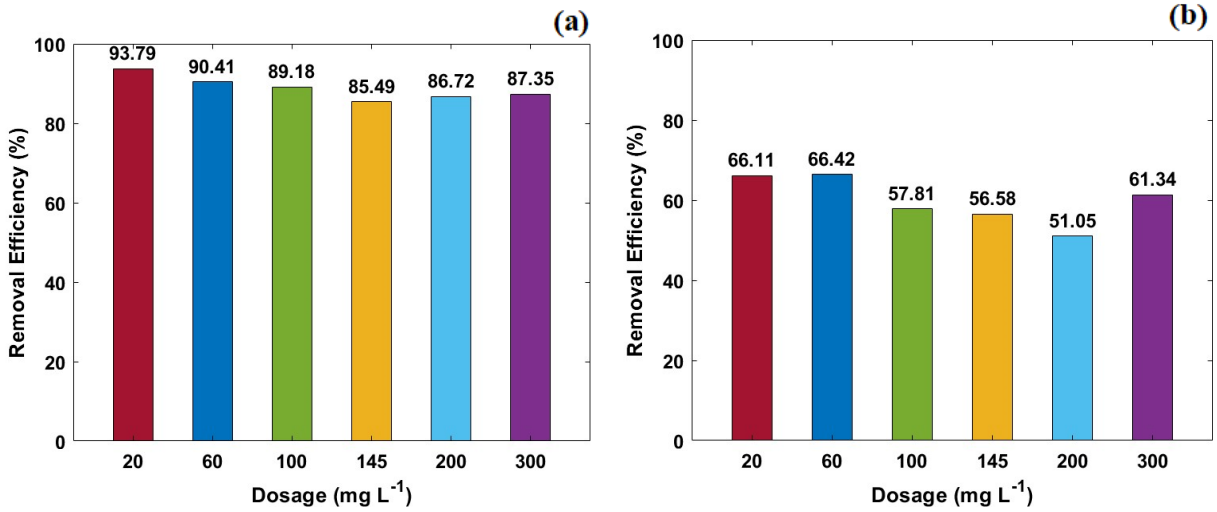

Figure 8: Effects of dosage (mg L^{-1}) on the removal efficiency of 20 mg L^{-1} PGS solution after 1 hour of treatment **(a)** and 2 hours of treatment **(b)**

After 2 hours of treatment, the removal efficiency declined dramatically, as shown in Figure 8b. What was once 93.79% removal efficiency for 20 mg L^{-1} after 1 hour has plummeted to 66.11% after 2 hours of treatment. Furthermore, a similar trend was observed at higher dosages of MoS_2.

It is also apparent in Figure 8b that as the MoS_2 dosage increased, a drop in the removal of PGS was observed; however, a slight recovery at 300 mg L^{-1} was made. This trend may indicate that higher dosages of MoS_2 may cause the nanoparticles to agglomerate, which would lower their effective surface area and activation sites, resulting in a lower removal efficiency. Furthermore, longer exposure times may also cause adsorbed PGS molecules to desorb from the surface of MoS_2, leading to a reduction in removal efficiency [115][72].

3.3 Effects of initial pH

pH has a significant influence on the removal efficiency of nanomaterials [116][117]. The effects of initial pH values on the effectiveness of PGS removal by MoS_2 nanoparticles were examined and the results are presented in Figure 9. In acidic conditions (pH 3 and pH 5) the removal efficiency after 1 hour, in Figure 9a, was quite similar, at 93.68% and 93.32%, respectively. Adsorption efficiency reached a maximum of 96.99% at pH of 7. This trend is also observed after 2 hours of treatment, as can be seen in Figure 9b. This indicates that neutral conditions represent the optimal pH for PGS adsorption onto MoS_2 nanoparticles. At pH 10, the removal efficiency dropped slightly after 1-hour and 2-hours, indicating that more alkaline conditions are not favorable for the removal of PGS. The fluctuations in removal efficiency at different pH levels could be due to changes in the surface charge of MoS_2 nanoparticles and the ionization state of PGS [118]. Furthermore, the slight decrease in removal efficiency at pH 10 could be due to MoS_2 nanoparticles' higher affinity towards hydroxide ions as opposed to PGS molecules [119]. Overall, this demonstrates that MoS_2 is effective at removing PGS under all acidic conditions.

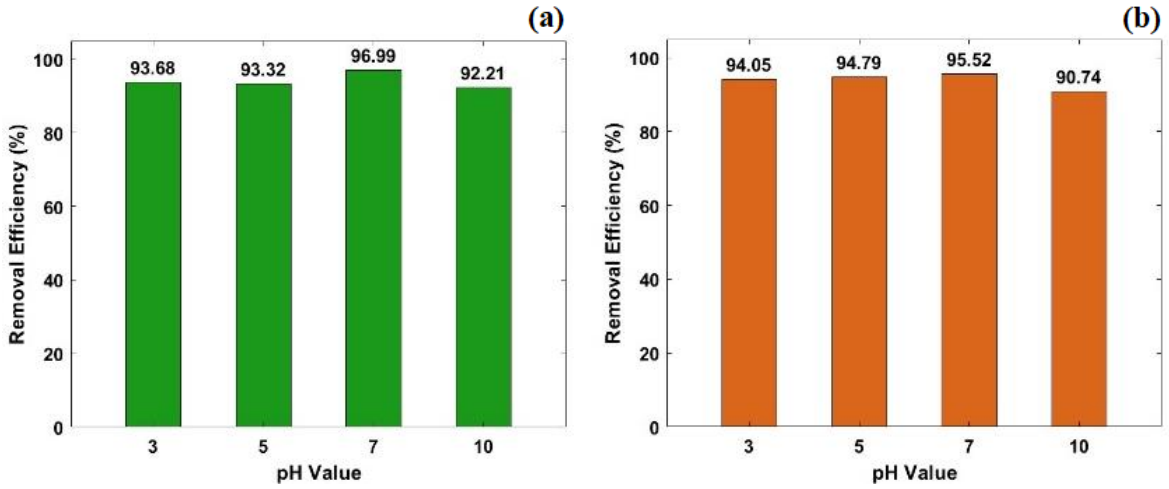

Figure 9: Removal efficiency of MoS2 in removing PGS for initial pH values of 3,5, 7 and 10 after 1 hour of treatment **(a)** and 2 hours of treatment **(b)**

3.4 Effects of initial concentration

The relationship between the initial concentration of PGS and the removal efficiency using 20 mg L^{-1} MoS_2 nanoparticles was investigated, and the results are depicted in Figure 10. On the left panel (Figure 10a), removal efficiency at individual initial PGS concentrations is represented after 1 hour of contact time. On the right side (Figure 10b), the removal efficiency was recorded at contact times of 5, 10, 15, 30, 60, 90, and 120 minutes for various initial PGS concentrations.

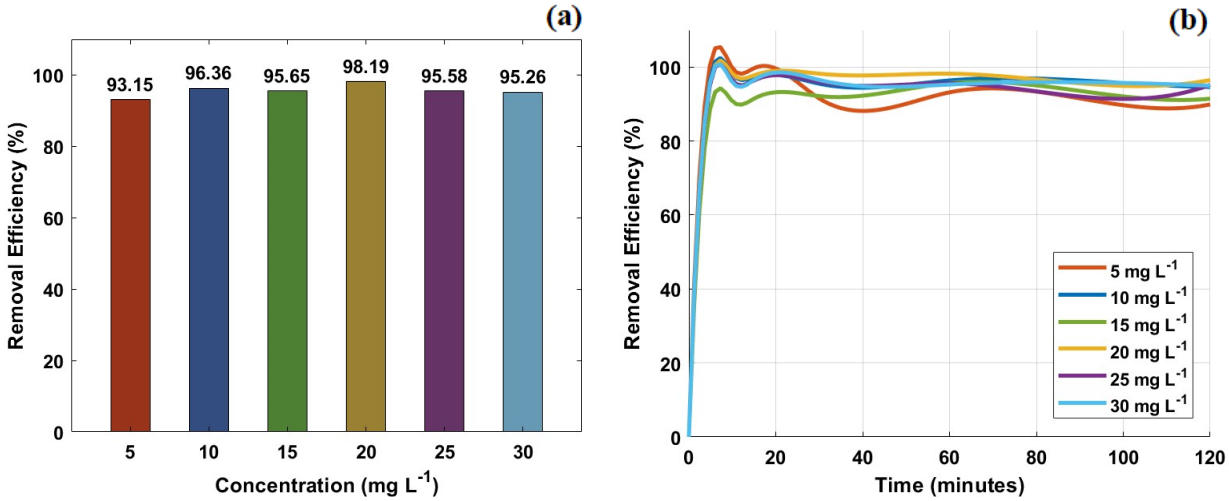

Figure 10: Effects of initial concentration of PGS (mg L^{-1}) on its removal using MoS_2 nanoparticles. **(a)** represents the removal efficiency after 1 hour of contact. **(b)** represents the removal efficiency of different initial PGS concentrations over time.

From Figure 10a, it is clear that the removal efficiency of MoS_2 is excellent across all initial PGS concentrations, ranging from 5 mg L^{-1} to 30 mg L^{-1}. At the lowest PGS concentration of 5 mg L^{-1}, the removal efficiency was at 93.15%. Further increases in PGS concentration did not significantly impact MoS_2 nanoparticle's ability to treat PGS until reaching a peak removal efficiency of 98.19% at 20 mg L^{-1} PGS. Beyond this concentration, the nanoparticles' performance decreased by around 2% after an additional 5 mg L^{-1} and stagnated at 30 mg L^{-1}. Figure 10b indicates that PGS is rapidly removed within the first 5 minutes of contact with MoS_2 nanoparticles and then gradually stabilizes, achieving a near-maximum removal efficiency within 60-80 minutes of contact for all tested concentrations. This rapid adsorption indicates that MoS_2 nanoparticles have a high affinity for PGS molecules. Furthermore, the subsequent stabilization in removal efficiency indicates that the adsorption sites on MoS_2 become saturated over time, leading to equilibrium and some desorption.

Overall, these results indicate that MoS_2 maintains high removal efficiency over time regardless of the initial PGS concentration.

3.5 Effects of temperature and thermodynamic analysis

The removal efficiency of PGS by MoS_2 nanoparticles was investigated at various temperatures and treatment durations. The results of this experiment are presented in Figure 11, which shows the removal efficiencies at temperatures of 25°C, 35°C, 45°C, and 55°C after 1 hour **(a)** and 2 hours **(b)** of treatment.

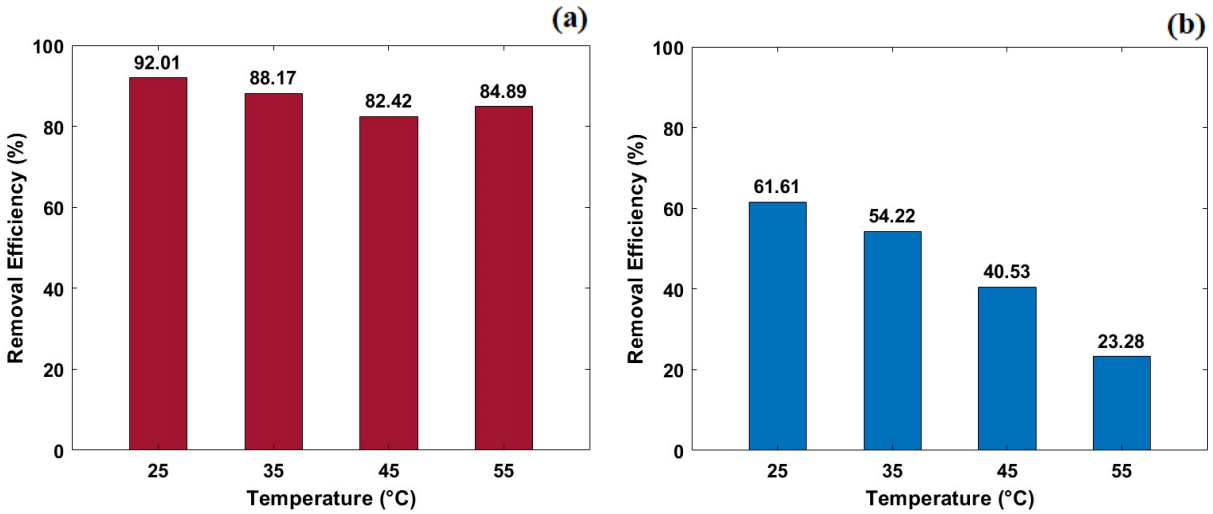

Figure 11: Removal efficiency of MoS_2 nanoparticles in treating PGS at temperatures of 25°C, 35°C, 45°C and 55°C after 1 hour **(a)** and 2 hours **(b)** of treatment.

In the left panel, the highest removal efficiency of 92.01% was observed at 25°C; however, as the treatment temperature gradually increased, the removal efficiency grew retrogressively. By increasing the temperature to 35°C, the removal efficiency dropped by 4.17% and then by another 6.52% at 45°C. At 55°C, the removal efficiency increased slightly to 84.89%. According to these results, PGS can be effectively removed by MoS_2 within an hour at all investigated temperatures, however, the optimal treatment temperature to achieve maximum removal efficiency is 25°C. It is possible that the fluctuation in PGS removal at higher temperatures could be attributed to a change in adsorption kinetics and surface interactions between PGS and MoS_2 nanoparticles [120]. Figure 11b illustrates the removal efficiency after 2 hours of contact. It can be seen that it reached a maximum removal efficiency of 61.61% at 25°C then subsequently decreased as the temperature increased. The lowest removal efficiency observed was at 55°C with a value of 23.28%. The results

presented for the 2-hours treatment time clearly indicate a trend of rapid decreasing removal efficiency with increasing temperature. This figure suggests that prolonged contact at higher temperatures negatively impacts the adsorption capacity of MoS_2 nanoparticles. This reduction in removal efficiency may be attributed to the potential desorption of adsorbed PGS molecules or potential alterations in the crystallinity or morphology of MoS_2 nanoparticles due to increased temperatures [115].

3.6 Reusability of MoS_2 nanoparticles for multiple adsorption cycles

A significant challenge of using adsorption mechanisms for wastewater treatment is the generation of sludge. However, reusing adsorbents significantly reduces sludge production [123][124]. To assess the sustained effectiveness of MoS_2 nanoparticles, their reusability over multiple adsorption cycles needs to be explored. The experiment involved subjecting MoS_2 nanoparticles to three consecutive adsorption cycles, as presented in Figure 12. Notably, the nanoparticles maintained a high and consistent removal efficiency throughout all cycles, demonstrating their reusability.

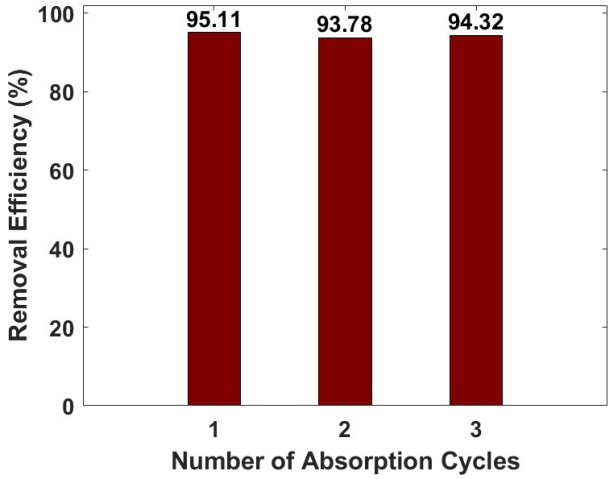

Figure 12: Reusability of MoS_2 nanoparticles for three PGS treatment cycles under the following adsorption conditions: Solution volume = 0.2 L, [PGS] = 20 mg L^{-1}, [MoS_2] = 20 mg L^{-1}, pH = 7, Temperature = 25°C, mixing rate = 1000 rpm, contact time = 1 hour.

MoS_2 nanoparticles' impressive reusable nature maintained a removal efficiency greater than 93% over the course of three treatment cycles. This demonstrates that it has the ability to reduce sludge generation, is cost-effective, and has high durability, making it ideal for field applications.

3.7 Removal mechanism of progesterone by MoS_2 nanoparticles

MoS_2 nanoparticles exhibited high removal efficiency of PGS in water across all experimental conditions. This suggest that several removal mechanisms are involved, and understanding these principles allows for further optimization of MoS_2 in water treatment applications. One of the primary mechanisms involved in the removal of PGS is adsorption. Adsorption is the process in which contaminants interacts with the surface of an adsorbent like MoS_2 due to its innate properties [123]. For one, the MoS_2 synthesized for this experiment has a relatively low surface area of 0.241 $m^2\ g^{-1}$ as demonstrated by the BET analysis. Comparatively, other studies reveal a surface area of 80 $m^2\ g^{-1}$ [114]. This could be due to the high agglomeration observed in Figure 6. However, this figure also depicts high porosity, which is challenging to measure using BET analysis, since these involve macropores that are greater than 50 nm in diameter, mesopores that are between 2-50 nm in diameter, and micropores that are below 2 nm in diameter as can be seen in Figure 13.

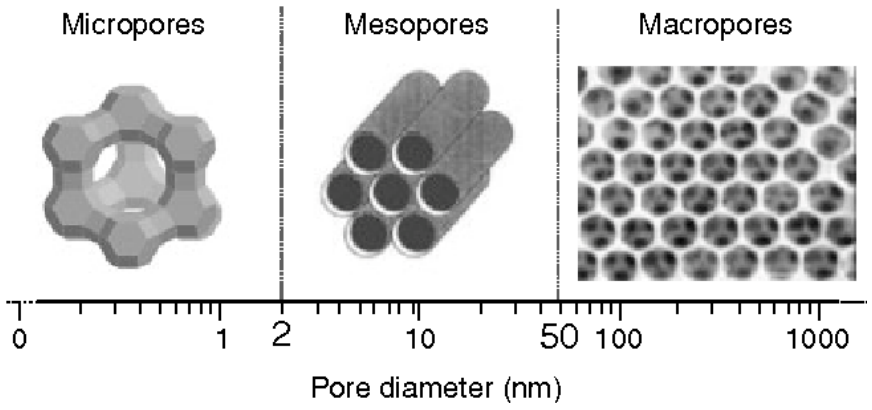

Figure 13: The IUPAC classification of porous materials on the basis of pore diameter. Porous inorganic materials. Adapted from Y. Wang and X. Bu, "Porous Inorganic Materials," Semantic Scholar. [Online]. Available: https://www.semanticscholar.org/paper/Porous-Inorganic-Materials-Wang-Bu/38f02dcb99418e7ff3a972c3c2370e18531fc628. Licensed under CC BY 4.0.

The nitrogen molecules used in the BET analysis may have difficulty accessing small micropores (<1 nm) due to kinetic restrictions at the operating temperatures [124]. Furthermore, narrow or complex pore structures may be unaccounted for in the BET analysis, leading to an underestimated surface area [127][128]. Additionally, adsorption can also occur by Van der Waals forces, which facilitate adsorption by inducing dipoles in the PGS molecules, leading to a weak but significant attraction [127]. Adsorption of PGS can also involve hydrogen bonding, as PGS contains

functional groups like hydroxyl and carbonyl groups that can participate in this bonding with interaction sites on MoS_2 nanoparticles [128].

Electrostatic interactions can also be a mechanism involved in the high removal efficiency of PGS, since MoS_2 nanoparticles possess a surface charge. These charged nanoparticles can then attract oppositely charged PGS molecules, especially if the pH conditions are favorable. Neutral pH conditions are most favorable in promoting adsorption interactions, while acidic and alkaline conditions can affect electrostatic interaction due to the surface charge of MoS_2 and the ionization state of PGS which could be seen in **Figure 9** [129][128]. Additionally, PGS is known to be a hydrophobic molecule, and MoS_2 exhibits hydrophobic properties [130][131]. This hydrophobic interaction between PGS and the nanoparticles' surface can further enhance its adsorption affinity, and this interaction is more significant at neutral pH conditions [132]. Furthermore, both PGS and MoS_2 contain π-electrons, which allow them to form $\pi - \pi$ bonds. These bonds can form between the aromatic rings of PGS and the surface of MoS_2. This bonding strengthens the adsorption process, increasing the overall removal efficiency [133]. The removal mechanism could also involve chemical interactions like coordination bonding due to the sulfur atoms in MoS_2. These sulfur atoms have the ability to interact with functional groups in PGS, thus forming stable complexes which promote adsorption. This chemical removal mechanism is also highly sensitive to pH and temperature, which is consistent with the results discussed in previous sections [134].

Lastly, the adsorption of PGS on the nanoparticles' surface is a dynamic process governed by equilibrium between sorption and desorption. This is well illustrated in Figure 11b. At first, PGS molecules are quickly adsorbed due to the availability of binding sites on MoS_2. After some time, these sites become occupied and an equilibrium state is achieved, where the rates of PGS sorption and desorption are balanced. This equilibrium state is influenced by many factors, such as dosage of MoS_2, reaction temperature, initial concentration of PGS, and initial pH conditions. In conclusion, the removal of PGS using MoS_2 is a complex process and could involve a synergistic removal mechanism. Furthermore, since Figure 12 indicates high MoS_2 nanoparticle reusability, it suggests that the removal mechanisms work synergistically. The most prominent removal mechanism will be further validated through future studies, including detailed isotherm analysis, determination of the point zero charge (PZC), and a comprehensive thermodynamic analysis. These investigations will provide deeper insight into the material's adsorption behaviour.

3.8 Kinetic analysis

This study investigated the adsorption kinetics of PGS using various kinetic models, including pseudo-first order (PFO), pseudo-second order (PSO), intraparticle diffusion and the Elovich model. The analysis focuses on PGS concentrations ranging from 5 to 30 mg L^{-1} and provides insight into the adsorption mechanism, which is crucial for improving PGS removal efficiency [135].

The PFO and PSO models are characterized by four key parameters, as depicted in Table 3. R^2 is the correlation coefficient, K_1 and K_2 are the rate constants for the PFO and PSO, respectively, q_e is the equilibrium adsorption capacity, and the AIC_C is the Akaike information criterion [136]. In the PFO model, the R^2 values range from 0.983 to 1.000, indicating a very good fit across all the tested PGS concentrations. The best fit, indicated by the highest R^2 value of 1.000, is observed at the highest PGS concentration of 30 mg L^{-1}. However, the AIC_c value for this concentration is the highest at 54.51, suggesting that the model may not be the most efficient fit for this data point.

Conversely, in the PSO model, the R^2 values range between 0.983 and 0.9997, also indicating an excellent fit across all concentrations. Similar to the PFO model, the R^2 value is highest for the 30 mg L^{-1} concentration, though slightly lower than that of the PFO model. The AIC_c values for the PSO model are generally competitive with those of the PFO model, suggesting that both models could be viable, though the PSO model shows slightly better overall correlation.

Table 3: Pseudo-first order and pseudo-second order models using experimental data and kinetic parameters.

Pseudo first-order model				
Initial PGS concentration (mg L^{-1})	K_1 (min^{-1})	q_e (mg · g^{-1})	R^2	AIC_c value
5	4.8701	44.54	0.983	27.66
10	3.3246	84.92	0.999	18.33
15	0.6648	100.52	0.998	24.94
20	0.8562	172.05	0.999	25.00
25	2.5230	184.48	0.998	31.00
30	2.4815	183.50	1.000	54.51

Pseudo second-order model				
Initial PGS concentration (mg L^{-1})	K_2 ($g \cdot mg^{-1} \cdot min^{-1}$)	q_e ($mg \cdot g^{-1}$)	R^2	AIC_c value
5	2.148E+06	44.54	0.983	27.66
10	3.376E+00	84.93	0.999	18.48
15	3.945E-02	101.52	0.999	22.62
20	1.935E-01	172.03	0.9991	26.22
25	2.016E+01	184.52	0.998	31.01
30	2.640E+00	183.54	0.9997	54.51

In the intraparticle diffusion model, the key parameters are K_{intra} (rate constant), C_{intra} (intercept representing the boundary layer effect), R^2 (correlation coefficient), and AIC_c (Akaike information criterion). Table 4 shows an R^2 range between 0.225 and 0.362, indicating a less-than-ideal fit. This implies that diffusion may not be the sole rate-limiting step in PGS adsorption. The highest R^2 value is observed at a PGS concentration of 15 mg L^{-1} (0.362), but overall, the model's low R^2 and high AIC_c values imply that the intraparticle diffusion model is not the most effective in describing the adsorption process. In addition, the Elovich kinetic parameters are presented in Table 4. In this model, the key parameters are α (initial adsorption rate), β (desorption constant), R^2 and AIC_c, as previously stated. The R^2 value in this model suggests a good fit across various concentrations, with values ranging from 0.579 to 0.995. The best fit, with an R^2 value of 0.995, is observed at the highest PGS concentration of 30 mg L^{-1}, though the AIC_c value is also highest at this concentration, suggesting some inefficiencies.

Overall, the PFO and PSO models show a very strong correlation in describing the PGS adsorption, both exhibiting high R^2 values and similar AIC_c values, a combination of physisorption and chemisorption mechanisms. Furthermore, the Elovich model demonstrates promising initial adsorption kinetics with a strong R^2 value across various PGS concentrations, particularly at higher concentrations. However, the intraparticle diffusion model appears less effective, with the lowest R^2 values, implying that diffusion is unlikely to be the primary adsorption mechanism in this interaction.

Table 4: Intraparticle diffusion and Elovich models using experimental data and kinetic parameters.

Intraparticle diffusion model				
Initial PGS concentration (mg L^{-1})	K_{intra} (mg · g^{-1} × $min^{1/2}$)	C_{intra} (mg · g^{-1})	R^2	AIC_c value
5	2.00	28.26	0.225	50.58
10	4.42	50.61	0.307	57.55
15	5.65	57.17	0.362	59.03
20	9.12	101.29	0.321	65.88
25	9.56	110.11	0.31	51.05
30	12.41	87.55	0.318	69.65
Elovich Model				
Initial PGS concentration (mg L^{-1})	α (mg · g^{-1} · min^{-1})	β (mg · g^{-1})	R^2	AIC_c value
5	32.43	0.1132	0.579	48.77
10	1.70E+05	0.1629	0.938	43.39
15	5.06E+04	0.1213	0.954	43.61
20	6.52E+06	0.0978	0.964	48.51
25	3.41E+06	0.0869	0.952	51.05
30	1.00E+23	0.3005	0.995	54.84

3.9 Storage of PGS and MoS_2

The material safety data sheet (MSDS) provided by TCI Co., Ltd., the manufacturer of the purchased PGS, describes specific storage guidelines to preserve the integrity and stability of PGS in its dry form [137]. The PGS was kept in its amber bottle to protect it from light, which can degrade the compound. The bottle was tightly sealed and placed in a dark refrigerator at a temperature of 3°C to prevent degradation and moisture absorption. The PGS stock solutions required different storage conditions. As illustrated in Figure 4, the storage of PGS solution is very important since it is highly sensitive to external factors such as temperature and light. Based on that experiment, the PGS solution showed stability on the first day at room temperature and cool conditions but became unstable in warm conditions. After day 1, the stability was significantly compromised across all storage conditions. It is best to use the PGS solution soon after preparation in order to preserve stability and ensure accurate results.

MoS_2 requires specific storage conditions as well to preserve its integrity and usability. The MoS_2 nanoparticles were stored at room temperature in a dark place, void of light, since light can potentially cause photooxidation [115]. The container was tightly sealed to prevent contamination, air exposure, and moisture, which may cause the nanoparticles to aggregate. All safety precautions, such as using personal protective equipment (PPE), were followed while handling, PGS, MoS_2 nanomaterial and other chemicals. The MSDS guidelines for safety and storage were strictly followed to ensure the integrity and safe use of MoS_2.

3.10 Performance analysis of MoS_2 nanoparticles and other Molybdenum-based nanomaterials

The performance of MoS_2 nanoparticles in the removal of PGS from water has been evaluated under several experimental conditions. To contextualize these findings, it is important to compare them with other molybdenum-based nanomaterials, although there have not been any studies specifically regarding the removal of PGS from water. Molybdenum trioxide (MoO_3) and molybdenum carbide (Mo_2C) have been selected for this performance comparison.

Firstly, MoO_3 nanoparticles, an oxide of molybdenum, are also widely used in a variety applications such as catalysis, optics, electrochemistry, and environmental remediation due to their unique properties [138]. Based on a study, MoO_3 was used as a catalyst in catalytic wet air

oxidation for the treatment of pharmaceutical wastewater containing a variety of pollutants including organic substances, pharmaceutical residues, solvent and other chemicals [139]. According to this study, it was used as a catalyst in high dosages to effectively degrade these contaminants from water. It achieved this by facilitating the degradation of water-borne contaminants through the production of hydroxyl radicals (OH) which exhibit strong oxidation properties under extreme conditions. Although MoO_3 was employed as a catalyst and not as a standalone adsorbent, its adsorption capacity is limited and has weaker hydrophobic interactions [140]. This demonstrates that MoS_2 is a superior nanomaterial for removing organic contaminants from water.

The next molybdenum-based product for comparison is Mo_2C nanoparticles. This nanoparticle has been seldom investigated for its application in environmental remediation, but it has been used in many applications, including semiconductors, electrocatalysis, and other industrial applications. Mo_2C possesses strong catalytic properties that promote hydrogenation and oxidation reactions [141]. These types of reactions can break down toxic organic pollutants into less harmful substances [142]. However, a major disadvantage of Mo_2C nanoparticles is that they are highly unstable in aqueous conditions, since they require specific conditions to maintain catalytic activity [141]. This is not very promising for environmental remediation since environmental factors are often unpredictable. This performance comparison unequivocally demonstrates the superior performance of MoS_2 nanoparticles for the efficient removal of organic contaminants from aqueous environments.

3.11 Economic evaluation of MoS_2 nanomaterials for environmental remediation

The economic feasibility of using MoS_2 nanoparticles to effectively remediate PGS-polluted water was analyzed. The analysis considered the cost of synthesizing MoS_2 nanoparticles at a large scale by sourcing the raw materials from the same providers presented in Table 1. This analysis was conducted using the prices retrieved on July 14, 2024, as summarized in Table 5. Other costs such as electricity and water were not included in this analysis. Additionally, no acids or bases are required since the optimal removal condition is at a neutral pH level. Based on Equation 1, and the reaction using 0.6 g of $(NH_4)_6MO_7O_{24} \cdot 4H_2O$ and 1.2 g of CH_4N_2S, the mass of MoS_2

theoretically produced using the hydrothermal synthesis method is approximately 0.544 g. The limiting reactant is $(NH_4)_6MO_7O_{24} \cdot 4H_2O$ since the molar ratio indicates excess thiourea.

Table 5: Cost analysis for treating water contaminated with PGS using MoS2 nanoparticles.

Price of $(NH_4)_6MO_7O_{24} \cdot 4H_2O$	Price of CH_4N_2S	Cost of 1g MoS_2 nanoparticles	Treatment cost by MoS_2
¥15,500/500 g (¥31.0/1g)	¥13,600/500 g (¥27.2/1g)	¥72.92	¥1.46/L

Given material costs of ¥31.0 per gram for ammonium molybdate tetrahydrate and ¥27.2 per gram for thiourea, the production cost for 1 g of MoS_2 is calculated to be ¥72.92 [143], [144]. Since the optimal MoS_2 dosage to treat an initial concentration of 20 mg L^{-1} of PGS is also 20 mg L^{-1}, we will use this dosage for the economic analysis. According to Table 5, the cost for this amount of MoS_2 to treat 1 L of PGS solution is: 0.02 g × ¥72.92/g = ¥1.46. Table 6 presents a cost comparison between MoS_2 and activated carbon for treating PGS, with MoS_2 being significantly more cost effective at 1.46 ¥ / L compared to 6.4 ¥ / L for activated carbon [52]. Additionally, the cost of using zero-valent iron (Fe^0) nanoparticles to treat the pharmaceutical ciprofloxacin is also included in Table 6 [145]. The data clearly shows that MoS_2 nanoparticles offer a more economically feasible option. The cost-effectiveness of MoS_2 nanoparticles is further enhanced by its ability to be regenerated and reused across multiple treatment cycles with minimal performance loss.

Table 6: Cost analysis of nanomaterials for treating pharmaceutical contamination in water.

Nanomaterial	Cost (¥ / g)	Dosage (mg L^{-1})	Treatment Cost (¥ / L)
MoS_2	72.92	20	1.46
Activated carbon	80.00	80	6.4
Fe nanoparticles	93.88	700	65.72

In conclusion, this analysis demonstrates that using MoS_2 for treating PGS-polluted water is economically viable, providing an effective and affordable solution for wastewater treatment.

3.12 Limitation and challenges

Despite the effectiveness of MoS_2 nanoparticles in removing PGS from water, there are always limitations and challenges when adopting new technologies. Firstly, scaling up the production of MoS_2 from laboratory scale to industrial scale may prove to be challenging and may also affect the economic feasibility. When scaling up the synthesis of a nanomaterial, ensuring uniform quality can be difficult to maintain due to some issues such as aggregation, degradation, and low production yield [146]. The hydrothermal method used in laboratory-scale synthesis produces small batches of nanomaterial, so scaling this up would require significant process optimization. Furthermore, each synthesized batch will contain inconsistencies, which leads to variability in its physical and chemical performance thus affecting its capacity for water treatment. The hydrothermal method utilizes an autoclave to provide high temperature and pressure promoting nucleation, crystallization, and growth of MoS_2 nanoparticles [147]. Manufacturing an industrial-scale autoclave would demand significant capital thus affecting the economic feasibility. Moreover, at this large scale, maintaining high temperature and pressure over an extended period of time would require a large amount of energy, negatively contributing to production costs and increasing the carbon footprint [148].

The stability and recovery of MoS_2 may also be affected when scaling up its manufacturing. The conditions at water treatment plants are subject to rapid change with the presence of other chemicals and contaminants, which may act as inhibitors or reduce the performance of the nanoparticle. Reclaiming MoS_2 nanoparticles from treated water may require additional resources and processes, like filtration and sedimentation, which can also increase operational costs. The incomplete recovery of these nanoparticles may lead to their release into the environment, potentially causing ecological damage and health risks; however their potential toxicity is not completely understood [149]. Lastly, water and wastewater treatment plants are considered continuous treatment systems. The performance of MoS_2 nanoparticles was only studied in a discrete system with isolated conditions and a controlled environment. Although MoS_2 demonstrated rapid kinetics and consistently high removal efficiency across different pH levels, dosages and treatment cycles, scaling the operational process would also require further optimization of these parameters to narrow down contact time, dosage, and flow rate [150].

Chapter 4

Conclusion

4.1 Summary of findings

Based on the results obtained, MoS_2 nanoparticles are very effective at adsorbing and removing PGS from aqueous environments, demonstrating adaptability across a variety of experimental conditions. There are numerous factors that affect the performance of MoS_2 in removing PGS from water. The optimal MoS_2 dosage achieved was 20 mg L^{-1}, with a significant removal rate of 93.79% in just 1 hour of contact. Increasing the dosage resulted in marginal improvements, but prolonged exposure can cause agglomeration and lower removal efficiency. Furthermore, pH level has a significant impact on the adsorption process; neutral conditions (pH 7) yielded a maximum removal efficiency of 96.99%. However, more acidic and basic conditions resulted in slight reduction in performance due to changes in the nanoparticle's surface charge and PGS ionization. Examination of the initial concentration of PGS revealed a negligible impact on its removal efficiency. MoS_2 exhibited strong performance at all PGS concentrations tested, with peak removal efficiency at 98.19% with 20 mg L^{-1}. However, higher concentrations can cause saturation of the adsorption sites and a gradual drop in removal efficiency. Furthermore, the adsorption process is highly influenced by temperature variability. 25°C was shown to be the ideal temperature to achieve the highest PGS removal. Higher temperatures cause desorption and changes to the characteristics of MoS_2, which reduces its ability to adsorb PGS. The economic feasibility of MoS_2 is highlighted by its low treatment cost compared to other nanomaterials, coupled with its ability to be regenerated and reused across multiple treatment cycles, making it a sustainable and cost-effective option for long-term application.

MoS_2 nanoparticles remove PGS through a variety of different mechanisms, which can be broadly categorized into predominantly physisorption and chemisorption. Among these are the active sites and high porosity that MoS_2 nanoparticles possess. Furthermore, Van der Waals forces and chemical interactions drive both physisorption and chemisorption processes. Additionally, MoS_2 nanoparticles' layered structure facilitates PGS molecule intercalation, which improves adsorption. Moreover, the removal process is aided by coordination bonds, hydrophobic interactions, π-π interactions, and electrostatic attractions between PGS and MoS_2. These processes, which are impacted by variables such as pH, temperature, and dosage, contribute to an effective PGS removal mechanism, indicating that MoS_2 is a promising material for water treatment.

4.2 Implications for water treatment

MoS_2 nanoparticles demonstrate exceptional efficiency in removing PGS from water, showcasing their potential as a high-performance adsorbent. Its abilities in removing PGS have been demonstrated by its steady performance in a variety of experimental conditions, such as changes in dosage, pH, initial concentration, temperature, and treatment cycles. The nanoparticle's excellent removal efficiency and rapid adsorption kinetics make it a good choice for real-world water treatment applications. Neutral pH, low treatment dosage, and near-room temperature conditions are consistent with desired treatment conditions at a water and wastewater treatment facility. Its high removal efficiency, even during extended treatment time, makes this material robust. No additional acid or base is required to adjust the pH, and there are no energy costs incurred for optimal temperature adjustment. Moreover, PGS is found in water sources at much lower concentrations in the ng L^{-1} and μg L^{-1} range. The high removal efficiency of MoS_2 was achieved at PGS concentrations in mg L^{-1}, which suggests that it will be even more effective at these trace concentrations. Therefore, MoS_2 performance is expected to remain high in natural water bodies with considerably lower PGS levels.

In terms of integrating this technology in a water treatment facility, MoS_2 would be best used in tertiary water treatment to remove organic pollutants, such as PPCPs and EDCs like PGS, from the water. MoS_2 is ideal for this stage since eliminating persistent contaminants is crucial before releasing the water to the environment and the general population. Furthermore, MoS_2 nanoparticles can be included in suspension systems or fixed-bed reactors to improve treatment efficiency by absorbing dissolved organic materials and tiny particles [151]. Moreover, sophisticated oxidation techniques or membrane filtration combined with MoS_2 can greatly improve water quality [152]. Overall, MoS_2 nanoparticles are very promising for the application in water treatment due to their high adsorption capacity at low dosage, versatility across various treatment conditions, reusability, ability to effectively remove PGS at high concentrations and potentially other contaminants without requiring additional pH adjustments or significant energy costs.

4.3 Future work

MoS_2 nanoparticles show great promise in treating PGS-contaminated water; however, further research and development are necessary to optimize their application and address potential limitations. To begin with, MoS_2 should be tested in the presence of other contaminants, coexisting cations, and anions to understand its selectivity and efficiency in more complex water matrices. It is also important that the nanomaterials do not strip essential minerals from water such as calcium, magnesium and potassium or trace elements like zinc and iron [153]. These tests will help determine the effects of ions and organic compounds on the adsorption capacity and kinetics of MoS_2 nanoparticles. This can be achieved by artificially simulating real-world water conditions or by collecting water samples from local rivers and water treatment plants. Furthermore, MoS_2 nanoparticles should also be tested for removing other COCs that are persistent in water and determine the exact removal mechanisms involved. Future work should also focus on scaling up from batch experiments to pilot-scale studies and eventually full-scale water treatment applications. This would involve the optimization of every step from synthesis, operation and regeneration/reuse. Extensive field tests are required to evaluate the performance and economic feasibility of using MoS_2 nanoparticles in real-world conditions. In order to guarantee the safe and responsible use of MoS_2 nanoparticles in water treatment, extensive studies on the health and environmental impacts are necessary. Comprehensive long-term investigations on the impacts on both aquatic ecosystems and human health are imperative.

References

[1] "The distribution of water on, in, and above the Earth | U.S. Geological Survey." Accessed: Mar. 01, 2024. [Online]. Available: https://www.usgs.gov/media/images/distribution-water-and-above-earth

[2] "What Percentage of the Earth's Water Is Drinkable?," WorldAtlas. Accessed: Feb. 28, 2024. [Online]. Available: https://www.worldatlas.com/articles/what-percentage-of-the-earth-s-water-is-drinkable.html

[3] H. H. Mitchell, T. S. Hamilton, F. R. Steggerda, and H. W. Bean, "THE CHEMICAL COMPOSITION OF THE ADULT HUMAN BODY AND ITS BEARING ON THE BIOCHEMISTRY OF GROWTH," *J. Biol. Chem.*, vol. 158, no. 3, pp. 625–637, May 1945, doi: 10.1016/S0021-9258(19)51339-4.

[4] "Water scarcity | UNICEF." Accessed: Mar. 01, 2024. [Online]. Available: https://www.unicef.org/wash/water-scarcity

[5] "The Future of Industrialization in a Post-Pandemic World: Industrial Development Report 2022," UNIDO. Accessed: Mar. 01, 2024. [Online]. Available: https://www.unido.org/news/future-industrialization-post-pandemic-world-industrial-development-report-2022

[6] D. Stengel, S. O'Reilly, and J. O'Halloran, "Contaminants and pollutants," in *The Ecology of Transportation: Managing Mobility for the Environment*, J. Davenport and J. L. Davenport, Eds., Dordrecht: Springer Netherlands, 2006, pp. 361–389. doi: 10.1007/1-4020-4504-2_15.

[7] "Water Pollution Definition - Types, Causes, Effects." Accessed: May 08, 2024. [Online]. Available: https://www.nrdc.org/stories/water-pollution-everything-you-need-know

[8] O. US EPA, "Radiation Sources and Doses." Accessed: Mar. 01, 2024. [Online]. Available: https://www.epa.gov/radiation/radiation-sources-and-doses

[9] J. V. Tarazona, “Pollution, Water,” in *Encyclopedia of Toxicology*, vol. 7, 2024, pp. 808–815.

[10] O. US EPA, “Types of Drinking Water Contaminants.” Accessed: Mar. 01, 2024. [Online]. Available: https://www.epa.gov/ccl/types-drinking-water-contaminants

[11] J. Israelachvili, “Interactions Involving Polar Molecules,” 2011, pp. 71–90. doi: 10.1016/B978-0-12-375182-9.10004-1.

[12] L. Hou, Z. Zhou, R. Wang, J. Li, F. Dong, and J. Liu, “Research on the Non-Point Source Pollution Characteristics of Important Drinking Water Sources,” *Water*, vol. 14, no. 2, Art. no. 2, Jan. 2022, doi: 10.3390/w14020211.

[13] R. Bouhlila and N. T. Hariga, “Identification of aquifer pollution’s point sources with the reciprocity principle,” *Sci. Rep.*, vol. 12, no. 1, p. 9968, Jun. 2022, doi: 10.1038/s41598-022-13795-w.

[14] H. I. Zeliger, “Chapter 5 - Water and soil pollution,” in *Oxidative Stress its mechanisms and impacts on human health and disease onset*, Academic Press, 2023, pp. 47–69.

[15] N. Tomczyk, L. Naslund, C. Cummins, E. V. Bell, P. Bumpers, and A. D. Rosemond, “Nonpoint source pollution measures in the Clean Water Act have no detectable impact on decadal trends in nutrient concentrations in U.S. inland waters,” *Ambio*, vol. 52, no. 9, pp. 1475–1487, Sep. 2023, doi: 10.1007/s13280-023-01869-6.

[16] O. US EPA, “Basic Information about Nonpoint Source (NPS) Pollution.” Accessed: Mar. 01, 2024. [Online]. Available: https://www.epa.gov/nps/basic-information-about-nonpoint-source-nps-pollution

[17] O. US EPA, “Contaminants of Emerging Concern including Pharmaceuticals and Personal Care Products.” Accessed: Mar. 01, 2024. [Online]. Available: https://www.epa.gov/wqc/contaminants-emerging-concern-including-pharmaceuticals-and-personal-care-products

[18] P. Loganathan, S. Vigneswaran, J. Kandasamy, A. K. Cuprys, Z. Maletskyi, and H. Ratnaweera, “Treatment Trends and Combined Methods in Removing Pharmaceuticals and

Personal Care Products from Wastewater—A Review," *Membranes*, vol. 13, no. 2, Art. no. 2, Feb. 2023, doi: 10.3390/membranes13020158.

[19] M. Taher, S. Al-Mutwalli, T. Sapmaz, and D. Koseoglu-Imer, "Potential and Performance of Biological Processes for Treatment of Pharmaceuticals and Personal Care Products in Wastewater," 2021, pp. 523–550. doi: 10.1016/B978-0-12-822956-9.00027-1.

[20] O. A. AL Falahi *et al.*, "Occurrence of pharmaceuticals and personal care products in domestic wastewater, available treatment technologies, and potential treatment using constructed wetland: A review," *Process Saf. Environ. Prot.*, vol. 168, pp. 1067–1088, Dec. 2022, doi: 10.1016/j.psep.2022.10.082.

[21] O. US EPA, "Overview of the Endocrine System." Accessed: Mar. 01, 2024. [Online]. Available: https://www.epa.gov/endocrine-disruption/overview-endocrine-system

[22] "Endocrine Disruptors," National Institute of Environmental Health Sciences. Accessed: Mar. 06, 2024. [Online]. Available: https://www.niehs.nih.gov/health/topics/agents/endocrine

[23] Q. U. Ain *et al.*, "Endocrine-Disrupting Chemicals: Occurrence and Exposure to the Human Being," in *Endocrine Disrupting Chemicals-induced Metabolic Disorders and Treatment Strategies*, M. S. H. Akash, K. Rehman, and M. Z. Hashmi, Eds., Cham: Springer International Publishing, 2021, pp. 113–123. doi: 10.1007/978-3-030-45923-9_7.

[24] S. Mesiano, "The Role of Progesterone in Pregnancy," in *Hormones and Pregnancy: Basic Science and Clinical Implications*, F. Mecacci, F. Petraglia, and M. Di Tommaso, Eds., Cambridge: Cambridge University Press, 2022, pp. 50–60. doi: 10.1017/9781009030830.006.

[25] M. Stefaniak, E. Dmoch-Gajzlerska, K. Jankowska, A. Rogowski, A. Kajdy, and R. B. Maksym, "Progesterone and Its Metabolites Play a Beneficial Role in Affect Regulation in the Female Brain," *Pharmaceuticals*, vol. 16, no. 4, Art. no. 4, Apr. 2023, doi: 10.3390/ph16040520.

[26] M. Schumacher, X. Zhu, and R. Guennoun, "3.11 - Progesterone: Synthesis, Metabolism, Mechanism of Action, and Effects in the Nervous System," in *Hormones, Brain and Behavior (Third Edition)*, D. W. Pfaff and M. Joëls, Eds., Oxford: Academic Press, 2017, pp. 215–244. doi: 10.1016/B978-0-12-803592-4.00054-7.

[27] V. Theis and C. Theiss, “Progesterone Effects in the Nervous System,” *Anat. Rec.*, vol. 302, no. 8, pp. 1276–1286, 2019, doi: 10.1002/ar.24121.

[28] S. H. Mellon and H. Vaudry, “Biosynthesis of neurosteroids and regulation of their synthesis,” *Int. Rev. Neurobiol.*, vol. 46, pp. 33–78, 2001, doi: 10.1016/s0074-7742(01)46058-2.

[29] D. B. Cooper and P. Patel, “Oral Contraceptive Pills,” in *StatPearls*, Treasure Island (FL): StatPearls Publishing, 2024. Accessed: Jul. 01, 2024. [Online]. Available: http://www.ncbi.nlm.nih.gov/books/NBK430882/

[30] Sehar Ezdi, Vladimíra Kantorová, Joseph Molitoris, Philipp Ueffing, and Mark Wheldon, “World Family Planning 2022,” United Nations, New York, 2022. Accessed: Jul. 01, 2024. [Online]. Available: https://www.un.org/development/desa/pd/sites/www.un.org.development.desa.pd/files/files/documents/2023/Feb/undesa_pd_2022_world-family-planning.pdf

[31] Ann Biddlecom, Vladimíra Kantorová, Stephen Kisambira, Petra Nahmias, and Hantamalala Rafalimanana, “Trends in Contraceptive Use Worldwide,” United Nations, New York, 2015. Accessed: Jul. 01, 2024. [Online]. Available: https://www.un.org/development/desa/pd/sites/www.un.org.development.desa.pd/files/undesa_pd_report_2015_trends_contraceptive_use.pdf

[32] S. Gidlöf, “Use of progesterone in female reproduction: tradition and trends,” *Acta Obstet. Gynecol. Scand.*, vol. 94, no. S161, pp. 1–2, 2015, doi: 10.1111/aogs.12775.

[33] R. Romero, A. Meyyazhagan, S. S. Hassan, G. W. Creasy, and A. Conde-Agudelo, “Vaginal Progesterone to Prevent Spontaneous Preterm Birth in Women With a Sonographic Short Cervix: The Story of the PREGNANT Trial,” *Clin. Obstet. Gynecol.*, vol. 67, no. 2, p. 433, Jun. 2024, doi: 10.1097/GRF.0000000000000867.

[34] M. J. Rocha and E. Rocha, “Synthetic Progestins in Waste and Surface Waters: Concentrations, Impacts and Ecological Risk,” *Toxics*, vol. 10, no. 4, Art. no. 4, Apr. 2022, doi: 10.3390/toxics10040163.

[35] H. R. Kasambala, M. J. Rwiza, and R. H. Mdegela, “Levels and distribution of progesterone in receiving waters and wastewaters of a growing urban area,” *Water Sci. Technol.*, vol. 80, no. 6, pp. 1107–1117, Sep. 2019, doi: 10.2166/wst.2019.350.

[36] T. Eggen and C. Vogelsang, “Chapter 7 - Occurrence and Fate of Pharmaceuticals and Personal Care Products in Wastewater,” in *Comprehensive Analytical Chemistry*, vol. 67, E. Y. Zeng, Ed., in Persistent Organic Pollutants (POPs): Analytical Techniques, Environmental Fate and Biological Effects, vol. 67. , Elsevier, 2015, pp. 245–294. doi: 10.1016/B978-0-444-63299-9.00007-7.

[37] C. Payus, C. John, V. L. Wan, T. W. Hsiang, and W. N. Kui, “Occurrence of Steroid Sex Hormone Progesterone in Influent andEffluent of Oxidation Pond and the River Outlet of Waste WaterTreatment Case Study,” *J. Environ. Sci. Technol.*, vol. 9, no. 5, pp. 399–406, Aug. 2016, doi: 10.3923/jest.2016.399.406.

[38] T. Manickum and W. John, “Occurrence, fate and environmental risk assessment of endocrine disrupting compounds at the wastewater treatment works in Pietermaritzburg (South Africa),” *Sci. Total Environ.*, vol. 468–469, pp. 584–597, Jan. 2014, doi: 10.1016/j.scitotenv.2013.08.041.

[39] H. Chang, Y. Wan, S. Wu, Z. Fan, and J. Hu, “Occurrence of androgens and progestogens in wastewater treatment plants and receiving river waters: Comparison to estrogens,” *Water Res.*, vol. 45, no. 2, pp. 732–740, Jan. 2011, doi: 10.1016/j.watres.2010.08.046.

[40] K. Zhang, Y. Zhao, and K. Fent, “Occurrence and Ecotoxicological Effects of Free, Conjugated, and Halogenated Steroids Including 17α-Hydroxypregnanolone and Pregnanediol in Swiss Wastewater and Surface Water,” *Environ. Sci. Technol.*, vol. 51, no. 11, pp. 6498–6506, Jun. 2017, doi: 10.1021/acs.est.7b01231.

[41] D. W. Kolpin *et al.*, “Pharmaceuticals, Hormones, and Other Organic Wastewater Contaminants in U.S. Streams, 1999−2000: A National Reconnaissance,” *Environ. Sci. Technol.*, vol. 36, no. 6, pp. 1202–1211, Mar. 2002, doi: 10.1021/es011055j.

[42] S. Wang, Z. Huo, J. Gu, and G. Xu, “Benzophenones and synthetic progestin in wastewater and sediment from farms, WWTPs and receiving surface water: distribution, sources,

and ecological risks," *RSC Adv.*, vol. 11, no. 50, pp. 31766–31775, Sep. 2021, doi: 10.1039/D1RA05333G.

[43] C. Zhong, K. Xiong, and X. Wang, "Effects of progesterone on the reproductive physiology in zebrafish," Jun. 07, 2017, *bioRxiv*. doi: 10.1101/147280.

[44] G. G. Nuñez, T. Gentile, S. N. Costantino, M. I. Sarchi, and S. M. Venturiello, "In vitro and in vivo effects of progesterone on Trichinella spiralis newborn larvae," *Parasitology*, vol. 131, no. 2, pp. 255–259, Aug. 2005, doi: 10.1017/S0031182005007468.

[45] A. V. Nalbandov, "Effect of Progesterone on Ovarian Morphology and on Embryonal Mortality in Pregnant Rats, Pigs, and Sheep," *Ann. N. Y. Acad. Sci.*, vol. 71, no. 5, pp. 580–587, 1958, doi: 10.1111/j.1749-6632.1958.tb54635.x.

[46] R. Petkam, R. L. Renaud, A. M. M. S. Freitas, A. V. M. Canario, and J. F. Leatherland, "In vitro metabolism of progesterone, androgens and estrogens by rainbow trout embryos," *Fish Physiol. Biochem.*, vol. 27, no. 1, pp. 117–128, Sep. 2002, doi: 10.1023/B:FISH.0000021867.71729.22.

[47] C. Biswas, S. Maity, M. Adhikari, A. Chatterjee, R. Guchhait, and K. Pramanick, "Pharmaceuticals in the Aquatic Environment and Their Endocrine Disruptive Effects in Fish," *Proc. Zool. Soc.*, vol. 74, no. 4, pp. 507–522, Dec. 2021, doi: 10.1007/s12595-021-00402-5.

[48] "Cómo actúa la progesterona sobre el sistema nervioso central," *Salud Ment.*, vol. 23, no. 2, pp. 42–48, Jan. 2000.

[49] T. Tang, T. Shi, D. Li, J. Xia, Q. Hu, and Y. Cao, "Adsorption Properties and Degradation Dynamics of Endocrine-Disrupting Chemical Levonorgestrel in Soils," *J. Agric. Food Chem.*, vol. 60, no. 16, pp. 3999–4004, Apr. 2012, doi: 10.1021/jf300479z.

[50] Eliane Zanella Fabbris and Keller Nicolini, "Detecção de progesterona em tecidos vegetais de lactuca sp. por espectroscopia de uv," Jan. 2017, doi: 10.21575/25254766msb2016vol1n2254.

[51] M. M. S. Yazdan, R. Kumar, and S. W. Leung, "The Environmental and Health Impacts of Steroids and Hormones in Wastewater Effluent, as Well as Existing Removal Technologies: A Review," *Ecologies*, vol. 3, no. 2, Art. no. 2, Jun. 2022, doi: 10.3390/ecologies3020016.

[52] F. Esmaeeli, S. A. Gorbanian, and N. Moazezi, “Removal of Estradiol Valerate and Progesterone using Powdered and Granular Activated Carbon from Aqueous Solutions,” *Int. J. Environ. Res.*, vol. 11, no. 5, pp. 695–705, Dec. 2017, doi: 10.1007/s41742-017-0060-0.

[53] B. Samir *et al.*, “Preparation and Modification of Activated Carbon for the Removal of Pharmaceutical Compounds via Adsorption and Photodegradation Processes: A Comparative Study,” *Appl. Sci.*, vol. 13, no. 14, Art. no. 14, Jan. 2023, doi: 10.3390/app13148074.

[54] A. S. Mestre, M. Campinas, R. M. C. Viegas, E. Mesquita, A. P. Carvalho, and M. J. Rosa, “Chapter 17 - Activated carbons in full-scale advanced wastewater treatment,” in *Advanced Materials for Sustainable Environmental Remediation*, D. Giannakoudakis, L. Meili, and I. Anastopoulos, Eds., Elsevier, 2022, pp. 433–475. doi: 10.1016/B978-0-323-90485-8.00001-1.

[55] P. K. Pandis *et al.*, “Key Points of Advanced Oxidation Processes (AOPs) for Wastewater, Organic Pollutants and Pharmaceutical Waste Treatment: A Mini Review,” *ChemEngineering*, vol. 6, no. 1, Art. no. 1, Feb. 2022, doi: 10.3390/chemengineering6010008.

[56] S. Singh and A. Garg, “12 - Advanced oxidation processes for industrial effluent treatment,” in *Advanced Oxidation Processes for Effluent Treatment Plants*, M. P. Shah, Ed., Elsevier, 2021, pp. 255–272. doi: 10.1016/B978-0-12-821011-6.00012-8.

[57] M. N. Arifin, R. Jusoh, H. Abdullah, N. Ainirazali, and H. D. Setiabudi, “Recent advances in advanced oxidation processes (AOPs) for the treatment of nitro- and alkyl-phenolic compounds,” *Environ. Res.*, vol. 229, p. 115936, Jul. 2023, doi: 10.1016/j.envres.2023.115936.

[58] “What are the advantages and disadvantages of ultrafiltration, nanofiltration and reverse osmosis membranes for water treatment? - RO AGUA Water Treatment Solutions.” Accessed: Jul. 03, 2024. [Online]. Available: https://www.roagua.com/news/what-are-the-advantages-and-disadvantages-of-ultrafiltration-nanofiltration-and-reverse-osmosis-membranes-for-water-treatment/, https://www.roagua.com/news/what-are-the-advantages-and-disadvantages-of-ultrafiltration-nanofiltration-and-reverse-osmosis-membranes-for-water-treatment/

[59] “Reverse Osmosis Water Benefits & Disadvantages,” Wastewater Digest. Accessed: Mar. 08, 2024. [Online]. Available: https://www.wwdmag.com/wastewater-treatment/news/10926022/reverse-osmosis-water-benefits-disadvantages

[60] A. Chatterjee and N. Afreen, “Soil fungi, Aspergillus niger NAAC, as environmental pollution clean-up agent against Progesterone: Remediation strategy and preparation of Bioformulation,” *Appl. Environ. Biotechnol.*, vol. 7, no. 2, Art. no. 2, Mar. 2023, doi: 10.26789/AEB.2022.02.003.

[61] F. Bertaux, S. Sosa-Carrillo, A. Fraisse, C. Aditya, M. Furstenheim, and G. Batt, “Enhancing bioreactor arrays for automated measurements and reactive control with ReacSight,” May 18, 2021, *bioRxiv*. doi: 10.1101/2020.12.27.424467.

[62] Phuong Ho, Christoph Westerwalbesloh, Eugen Kaganovitch, Alexander Grünberger, and Peter Neubauer, “Reproduction of Large-Scale Bioreactor Conditions on Microfluidic Chips,” *Microorganisms*, vol. 7, no. 4, p. 105, Apr. 2019, doi: https://doi.org/10.3390/microorganisms7040105.

[63] “Transition Metal Dichalcogenide - an overview | ScienceDirect Topics.” Accessed: Mar. 05, 2024. [Online]. Available: https://www.sciencedirect.com/topics/materials-science/transition-metal-dichalcogenide

[64] K. Dreva, A. Morina, L. Yang, and A. Neville, “The effect of temperature on water desorption and oxide formation in MoS2 coatings and its impact on tribological properties,” *Surf. Coat. Technol.*, vol. 433, p. 128077, Mar. 2022, doi: 10.1016/j.surfcoat.2021.128077.

[65] O. Samy, S. Zeng, M. D. Birowosuto, and A. El Moutaouakil, “A Review on MoS2 Properties, Synthesis, Sensing Applications and Challenges,” *Crystals*, vol. 11, no. 4, Art. no. 4, Apr. 2021, doi: 10.3390/cryst11040355.

[66] Md. Ahmaruzzaman and V. Gadore, “MoS2 based nanocomposites: An excellent material for energy and environmental applications,” *J. Environ. Chem. Eng.*, vol. 9, no. 5, p. 105836, Oct. 2021, doi: 10.1016/j.jece.2021.105836.

[67] M. Saliba, J. P. Atanas, T. M. Howayek, and R. Habchi, “Molybdenum disulfide, exfoliation methods and applications to photocatalysis: a review,” *Nanoscale Adv.*, vol. 5, no. 24, pp. 6787–6803, Dec. 2023, doi: 10.1039/D3NA00741C.

[68] H. Zhang *et al.*, “Two-dimensional metal-phase layered molybdenum disulfide for electrocatalytic hydrogen evolution reaction,” *Nanoscale*, vol. 15, no. 9, pp. 4429–4437, Mar. 2023, doi: 10.1039/D2NR06184H.

[69] Y. Zhao, X. Zheng, P. Gao, and H. Li, “Recent advances in defect-engineered molybdenum sulfides for catalytic applications,” *Mater. Horiz.*, vol. 10, no. 10, pp. 3948–3999, Oct. 2023, doi: 10.1039/D3MH00462G.

[70] K. Wang, Q. Han, B. Chen, B. Liu, and Z. Wang, “Electrochemical exfoliation of MoS2 nanosheets with ultrahigh stability for lead adsorption,” *J. Water Process Eng.*, vol. 50, p. 103212, Dec. 2022, doi: 10.1016/j.jwpe.2022.103212.

[71] Y.-Z. Yao, Y.-J. Shi, and K.-H. Hu, “Preparation of Molybdenum Disulfide with Different Nanostructures and Its Adsorption Performance for Copper (II) Ion in Water,” *Nanomaterials*, vol. 13, no. 7, Art. no. 7, Jan. 2023, doi: 10.3390/nano13071194.

[72] L. O. Amaral and A. L. Daniel-da-Silva, “MoS2 and MoS2 Nanocomposites for Adsorption and Photodegradation of Water Pollutants: A Review,” *Molecules*, vol. 27, no. 20, Art. no. 20, Jan. 2022, doi: 10.3390/molecules27206782.

[73] Y. Tang, X. Zhang, P. Choi, Z. Xu, and Q. Liu, “Contributions of van der Waals Interactions and Hydrophobic Attraction to Molecular Adhesions on a Hydrophobic MoS2 Surface in Water,” *Langmuir*, vol. 34, no. 47, pp. 14196–14203, Nov. 2018, doi: 10.1021/acs.langmuir.8b02636.

[74] E. K. Shokr, H. A. Mohamed, H. A. Mohamed, M. S. Kamel, and H. M. Ali, “Enhancing the MoS2/MoO3/ZnS/Zn-Heterojunction catalyst’s photocatalytic performance for water organic pollutants,” *Phys. Scr.*, vol. 98, no. 8, p. 085917, Jul. 2023, doi: 10.1088/1402-4896/ace2ff.

[75] S. Li *et al.*, “Mo-Based Heterogeneous Interface and Sulfur Vacancy Synergistic Effect Enhances the Fenton-like Catalytic Performance for Organic Pollutant Degradation,” *ACS Appl. Mater. Interfaces*, vol. 15, no. 1, pp. 1326–1338, Jan. 2023, doi: 10.1021/acsami.2c19243.

[76] X. Kong *et al.*, “Insights into Adsorption Mechanisms of Nitro Polycyclic Aromatic Hydrocarbons on Common Microplastic Particles: Experimental Studies and Modeling,” Aug. 05, 2022, *Rochester, NY*: 4182808. doi: 10.2139/ssrn.4182808.

[77] Z. Wang *et al.*, “Boosting CO2 Hydrogenation to Formate over Edge-Sulfur Vacancies of Molybdenum Disulfide,” *Angew. Chem. Int. Ed.*, vol. 62, no. 45, p. e202307086, 2023, doi: 10.1002/anie.202307086.

[78] Kumari Prajakta, V. P. Vinturaj, Rohit Singh, Vivek Garg, and Saurabh Kumar Pandey, “Effect of Introducing Defects and Doping on Different Properties of Monolayer MoS2,” *Basic Solid State Phys.*, Jun. 2023, doi: https://doi.org/10.1002/pssb.202300017.

[79] S. McDonnell, R. Addou, C. Buie, R. M. Wallace, and C. L. Hinkle, “Defect-Dominated Doping and Contact Resistance in MoS2,” *ACS Nano*, vol. 8, no. 3, pp. 2880–2888, Mar. 2014, doi: 10.1021/nn500044q.

[80] K. Zhang *et al.*, “Manganese Doping of Monolayer MoS2: The Substrate Is Critical,” *Nano Lett.*, vol. 15, no. 10, pp. 6586–6591, Oct. 2015, doi: 10.1021/acs.nanolett.5b02315.

[81] S. García-Dalí, J. I. Paredes, S. Villar-Rodil, A. Martínez-Jódar, A. Martínez-Alonso, and J. M. D. Tascón, “Molecular Functionalization of 2H-Phase MoS2 Nanosheets via an Electrolytic Route for Enhanced Catalytic Performance,” *ACS Appl. Mater. Interfaces*, vol. 13, no. 28, pp. 33157–33171, Jul. 2021, doi: 10.1021/acsami.1c08850.

[82] S. M. Roopan and M. A. Khan, “Polymer-MoS2-metal oxide composite: An eco-friendly material for wastewater treatment,” in *Renewable Polymers and Polymer-Metal Oxide Composites*, S. Haider and A. Haider, Eds., in Metal Oxides. , Elsevier, 2022, pp. 165–193. doi: 10.1016/B978-0-323-85155-8.00002-9.

[83] A. Jawaid *et al.*, “Mechanism for Liquid Phase Exfoliation of MoS2,” *Chem. Mater.*, vol. 28, no. 1, pp. 337–348, Jan. 2016, doi: 10.1021/acs.chemmater.5b04224.

[84] M. A. Lukowski, A. S. Daniel, F. Meng, A. Forticaux, L. Li, and S. Jin, “Enhanced Hydrogen Evolution Catalysis from Chemically Exfoliated Metallic MoS2 Nanosheets,” *J. Am. Chem. Soc.*, vol. 135, no. 28, pp. 10274–10277, Jul. 2013, doi: 10.1021/ja404523s.

[85] C. Liu, Q. Wang, F. Jia, and S. Song, “Adsorption of heavy metals on molybdenum disulfide in water: A critical review,” *J. Mol. Liq.*, vol. 292, p. 111390, Oct. 2019, doi: 10.1016/j.molliq.2019.111390.

[86] B. Joshi, A. M. E. Khalil, S. Zhang, F. A. Memon, and Z. Yang, “Application of 2D MoS2 Nanoflower for the Removal of Emerging Pollutants from Water,” *ACS Eng. Au*, vol. 3, no. 6, pp. 461–476, Dec. 2023, doi: 10.1021/acsengineeringau.3c00032.

[87] Ayesha Zafir and Naheed Banu, “Modulation of in vivo oxidative status by exogenous corticosterone and restraint stress in rats.,” *Stress*, vol. 12, no. 2, pp. 167–177, Jul. 2009, doi: 10.1080/10253890802234168.

[88] X. Zhou, D. Wu, Z. Jin, X. Song, X. Wang, and S. L. Suib, “Significantly increased Raman enhancement on defect-rich O-incorporated 1T-MoS2 nanosheets,” *J. Mater. Sci.*, vol. 55, no. 34, pp. 16374–16384, Dec. 2020, doi: 10.1007/s10853-020-05172-7.

[89] “X線回折.” Accessed: Jul. 07, 2024. [Online]. Available: https://rigaku.com/ja/resources/techniques/x-ray-diffraction-xrd

[90] K. Thamaphat, P. Limsuwan, and B. Ngotawornchai, “Phase Characterization of TiO2 Powder by XRD and TEM”.

[91] “Bragg law | Definition, Equation, Diagram, & Facts | Britannica.” Accessed: May 02, 2024. [Online]. Available: https://www.britannica.com/science/Bragg-law

[92] “2.3: BET Surface Area Analysis of Nanoparticles,” Chemistry LibreTexts. Accessed: May 07, 2024. [Online]. Available: https://chem.libretexts.org/Bookshelves/Analytical_Chemistry/Physical_Methods_in_Chemistry_and_Nano_Science_(Barron)/02%3A_Physical_and_Thermal_Analysis/2.03%3A_BET_Surface_Area_Analysis_of_Nanoparticles

[93] “Scanning Electron Microscopy (SEM) Analysis and Imaging.” Accessed: Jun. 07, 2024. [Online]. Available: https://www.twi-global.com/what-we-do/services-and-support/failure-analysis-and-repair/microscopy/scanning-electron-microscopy-sem-analysis-and-imaging.aspx

[94] S. R. Cook, “Warp-Free TEM Sample Preparation Methods Using FIB/SEM Systems,” *Microsc. Microanal.*, vol. 28, no. 6, pp. 1961–1970, Dec. 2022, doi: 10.1017/s1431927622012181.

[95] O. Eljamal, A. M. E. Khalil, Y. Sugihara, and N. Matsunaga, “Phosphorus removal from aqueous solution by nanoscale zero valent iron in the presence of copper chloride,” *Chem. Eng. J.*, vol. 293, pp. 225–231, Jun. 2016, doi: 10.1016/j.cej.2016.02.052.

[96] K. Simeonidis and S. Mourdikoudis, Eds., *Nanoparticles as Sustainable Environmental Remediation Agents*. Royal Society of Chemistry, 2023. doi: 10.1039/9781837670215.

[97] A. M. E. Khalil, R. Eljamal, Y. Sugihara, and N. Matsunaga, “Treatment and Regeneration of Nano-scale Zero-valent Iron Spent in Water Remediation | 九大コレクション | 九州大学附属図書館”, Accessed: Jul. 22, 2024. [Online]. Available: https://hdl.handle.net/2324/1808449

[98] M. S. Islam, I. Maamoun, O. Falyouna, O. Eljamal, and B. B. Saha, “Arsenic removal from contaminated water utilizing novel green composite *Chlorella vulgaris* and nano zero-valent iron,” *J. Mol. Liq.*, vol. 370, p. 121005, Jan. 2023, doi: 10.1016/j.molliq.2022.121005.

[99] O. Falyouna, I. Maamoun, K. Bensaida, A. Tahara, Y. Sugihara, and O. Eljamal, “Chemical deposition of iron nanoparticles (Fe0) on titanium nanowires for efficient adsorption of ciprofloxacin from water,” *Water Pract. Technol.*, vol. 17, no. 1, pp. 75–83, Sep. 2021, doi: 10.2166/wpt.2021.091.

[100] K. Aoki, V. Giovangigli, and M. Hattori, “A kinetic model of adsorption on solid surfaces,” presented at the AIP Conference, Victoria BC: AIP Publishing LLC, Nov. 2016, p. 100005. doi: 10.1063/1.4967616.

[101] Md. M. Rahman, S. C. Karmaker, A. Pal, O. Eljamal, and B. B. Saha, “Statistical techniques for the optimization of cesium removal from aqueous solutions onto iron-based nanoparticle-zeolite composites,” *Environ. Sci. Pollut. Res.*, vol. 28, no. 10, pp. 12918–12931, Mar. 2021, doi: 10.1007/s11356-020-11258-1.

[102] T. Shahwan, “Lagergren equation: Can maximum loading of sorption replace equilibrium loading?,” *Chem. Eng. Res. Des.*, vol. 96, pp. 172–176, Apr. 2015, doi: 10.1016/j.cherd.2015.03.001.

[103] S. Lagergren, “About the Theory of So-Called Adsorption of Soluble Substances,” Accessed: Jul. 21, 2024. [Online]. Available: https://www.semanticscholar.org/paper/About-the-Theory-of-So-Called-Adsorption-of-Soluble-Lagergren/df4550de8be537d20199609ae668af1048a34ffb

[104] M. F. Idham, O. Falyouna, R. Eljamal, I. Maamoun, and O. Eljamal, “Chloramphenicol removal from water by various precursors to enhance graphene oxide–iron nanocomposites,” *J. Water Process Eng.*, vol. 50, p. 103289, Dec. 2022, doi: 10.1016/j.jwpe.2022.103289.

[105] G. Blanchard, M. Maunaye, and G. Martin, “Removal of heavy metals from waters by means of natural zeolites,” *Water Res.*, vol. 18, no. 12, pp. 1501–1507, Jan. 1984, doi: 10.1016/0043-1354(84)90124-6.

[106] Hui Qiu, Bing-cai Pan, Qing-jian Zhang, and Wei-ming Zhang, “Critical review in adsorption kinetic models,” *J. Zhejiang Univ.*, vol. 10, pp. 716–724, May 2009.

[107] F.-C. Wu, R.-L. Tseng, and R.-S. Juang, “Initial behavior of intraparticle diffusion model used in the description of adsorption kinetics,” *Chem. Eng. J.*, vol. 153, no. 1, pp. 1–8, Nov. 2009, doi: 10.1016/j.cej.2009.04.042.

[108] Sanjay Jatav, Kaline P. Furlan, Junying Liu, and Eric H. Hill, “Heterostructured Monolayer MoS2 Nanoparticles toward Water-Dispersible Catalysts,” *ACS Appl. Mater. Interfaces*, vol. 12, no. 17, pp. 19813–19822, Apr. 2020, doi: 10.1021/ACSAMI.0C02246.

[109] Getachew Solomon, Mojtaba Gilzad Kohan, Raffaello Mazzaro, Matteo Jugovac, and Paolo Moras, “MoS2 Nanosheets Uniformly Anchored on NiMoO4 Nanorods, a Highly Active Hierarchical Nanostructure Catalyst for Oxygen Evolution Reaction and Pseudo-Capacitors,” *Adv. Sustain. Syst.*, vol. 7, no. 2, pp. 2200410–2200410, Dec. 2022, doi: 10.1002/adsu.202200410.

[110] Harini Karthick, Koyeli Girigoswami, Pragya Pallavi, and Agnishwar Girigoswami, “MoS2 nanocomposites for biomolecular sensing, disease monitoring, and therapeutic applications,” *Nano Futur.*, vol. 7, no. 3, Jul. 2023, doi: 10.1088/2399-1984/ace178.

[111] Dhirendra Sahoo, Birendra Kumar, Jaivardhan Sinha, Subhasis Ghosh, Susanta Sinha Roy, and Bhaskar Kaviraj, “Cost effective liquid phase exfoliation of MoS2 nanosheets and photocatalytic activity for wastewater treatment enforced by visible light | Scientific Reports,” *Sci. Rep.*, vol. 10, no. 10759, Jul. 2020, Accessed: Jul. 09, 2024. [Online]. Available: https://www.nature.com/articles/s41598-020-67683-2

[112] N. Kumar *et al.*, “Probing on crystallographic structural and surface morphology of hydrothermally synthesized MoS2 nanoflowers consisting of nanosheets,” *Appl. Surf. Sci. Adv.*, vol. 6, p. 100167, Dec. 2021, doi: 10.1016/j.apsadv.2021.100167.

[113] G. Habibi Jetani and M. B. Rahmani, “Exploring the effect of hydrothermal precursor pH on the photosensitivity of 1T/2H–MoS2 nanosheets,” *Opt. Mater.*, vol. 124, p. 111974, Feb. 2022, doi: 10.1016/j.optmat.2022.111974.

[114] S. Sangeethavanathi, P. Gowthaman, S. Vigneswaran, and M. Sathishkumar, “Exploring the Structural, Optical and Surface Area Properties of Mos2 Nanoparticles – Material Science Research India,” *Mater. Sci. Res. India*, May 2024, Accessed: May 09, 2024. [Online]. Available: https://www.materialsciencejournal.org/vol21no2/exploring-the-structural-optical-and-surface-area-properties-of-mos2-nanoparticles/

[115] “Identifying the suitability of MoS2 nanoparticles by two different methods for Photo catalytic Applications,” *Int. J. Nanosci.*, Dec. 2022, doi: 10.1142/s0219581x23500060.

[116] Eduardo Leiva, Camila Tapia, and Carolina Rodríguez, “Removal of Mn(II) from Acidic Wastewaters Using Graphene Oxide–ZnO Nanocomposites,” *Molecules*, vol. 26, no. 9, May 2021, doi: https://doi.org/10.3390/molecules26092713.

[117] Eduardo Leiva, Camila Tapia, and Carolina Rodríguez, “Highly Efficient Removal of Cu(II) Ions from Acidic Aqueous Solution Using ZnO Nanoparticles as Nano-Adsorbents,” *Water*, vol. 13, no. 21, Oct. 2021, doi: https://doi.org/10.3390/w13212960.

[118] X. Wang, P. Zhang, F. Xu, B. Sun, G. Hong, and L. Bao, “Adsorption of Methylene Blue on Azo Dye Wastewater by Molybdenum Disulfide Nanomaterials,” *Sustainability*, vol. 14, no. 13, Art. no. 13, Jan. 2022, doi: 10.3390/su14137585.

[119] R. Qu *et al.*, “A MoS2 nanosheet-coated mesh for pH-induced multi-pollutant water remediation with in situ electrocatalysis,” *J. Mater. Chem. A*, vol. 6, no. 15, pp. 6435–6441, Apr. 2018, doi: 10.1039/C8TA00685G.

[120] J. Zhou, C. Si, and H. Gao, “The Adsorption Performance of MoS2 Nano-rod by Combined with Graphene Oxide for Cr(VI) Removal from Aqueous Solution,” *Mater. Sci.*, vol. 28, no. 1, Art. no. 1, Feb. 2022, doi: 10.5755/j02.ms.25269.

[121] Abu Zahrim Yaser, Afiq Iqmal Haqim, and Joshua Rechard Mijong, “Water Treatment Sludge as Coagulant and Adsorbent: A Recent Review | SpringerLink,” in *5th International Symposium on Water Pollution and Treatment*, Bangkok, Thailand: Springer, Sep. 2023, pp. 1–7. doi: DOI https://doi.org/10.1007/978-981-99-3737-0_1.

[122] R. Eljamal, I. Maamoun, K. Bensaida, G. Yilmaz, Y. Sugihara, and O. Eljamal, “A novel method to improve methane generation from waste sludge using iron nanoparticles coated with magnesium hydroxide,” *Renew. Sustain. Energy Rev.*, vol. 158, p. 112192, Apr. 2022, doi: 10.1016/j.rser.2022.112192.

[123] Douglas M. Ruthven, “Chapter 3,” in *Fundamentals of adsorption equilibrum and kinetics in microporous solids*, vol. 7, Molecular Sieves, 1998, pp. 31–65. doi: 10.1016/B978-075061959-2/50004-5.

[124] Joaquín Silvestre-Albero, Ana M. Silvestre-Albero, Philip L. Llewellyn, and Francisco Rodríguez-Reinoso, “High-Resolution N2 Adsorption Isotherms at 77.4 K: Critical Effect of the He Used During Calibration,” *J. Phys. Chem. C*, vol. 117, no. 33, pp. 16885–16889, Aug. 2013, doi: 10.1021/JP405719A.

[125] G. Ledezma, J. J. Verstraete, L. Sorbier, D. L.-L. Cocq, E. Jolimaitre, and C. Jallut, “Computational Characterization of a Pore Network Model by Using a Fast Nitrogen Porosimetry Simulation,” in *Computer Aided Chemical Engineering*, vol. 50, M. Türkay and R.

Gani, Eds., in 31 European Symposium on Computer Aided Process Engineering, vol. 50. , Elsevier, 2021, pp. 1111–1116. doi: 10.1016/B978-0-323-88506-5.50171-6.

[126] F. Liang *et al.*, "Pore Structure in Shale Tested by Low Pressure N2 Adsorption Experiments: Mechanism, Geological Control and Application," *Energies*, vol. 15, no. 13, Art. no. 13, Jan. 2022, doi: 10.3390/en15134875.

[127] Y. Andersson, D. C. Langreth, and B. I. Lundqvist, "Van der Waals interactions in density-functional theory: implementation and applications," *Phys. Rev. Lett.*, vol. 76, no. 102, Jan. 1996, doi: https://doi.org/10.1103/PhysRevLett.76.102.

[128] J. J. Gamboa-Carballo *et al.*, "Theoretical study of chlordecone and surface groups interaction in an activated carbon model under acidic and neutral conditions," *J. Mol. Graph. Model.*, vol. 65, pp. 83–93, Apr. 2016, doi: 10.1016/j.jmgm.2016.02.008.

[129] A. Ferino-Pérez, J. J. Gamboa-Carballo, Z. Li, L. C. Campos, and U. Jáuregui-Haza, "Explaining the interactions between metaldehyde and acidic surface groups of activated carbon under different pH conditions," *J. Mol. Graph. Model.*, vol. 90, pp. 94–103, Jul. 2019, doi: 10.1016/j.jmgm.2019.04.006.

[130] M. Alizadeh Noghani and D. E. Brooks, "Progesterone binding nano-carriers based on hydrophobically modified hyperbranched polyglycerols.," *Nanoscale*, vol. 8, no. 9, pp. 5189–5199, Feb. 2016, doi: 10.1039/C5NR08175K.

[131] Maryam Samanian and Mohammad Hadi Ghatee, "Wettability Scope of MoS2-Ionic Liquid Interfaces and Their Modification toward Novel Superhydrophobic Boundaries.," *Langmuir*, vol. 38, no. 15, pp. 4555–4566, Apr. 2022, doi: 10.1021/acs.langmuir.1c03227.

[132] L. Zhang *et al.*, "Superhydrophobic Nanoparticles: An Efficiently Selective Adsorbent for Surfactant-Like Contaminants from Complex Wastewater Matrices," *Small*, vol. 20, no. 5, p. 2305807, 2024, doi: 10.1002/smll.202305807.

[133] X. Liu *et al.*, "Efficient Adsorbent Derived from Phytolith-Rich Ore for Removal of Tetracycline in Wastewater," *ACS Omega*, vol. 9, no. 7, pp. 8287–8296, Feb. 2024, doi: 10.1021/acsomega.3c09049.

[134] H. Liu *et al.*, “3d transition metal coordination on monolayer MoS2: a facile doping method to functionalize surfaces,” *Nanoscale*, vol. 14, no. 30, pp. 10801–10815, Aug. 2022, doi: 10.1039/D2NR01132H.

[135] O. Eljamal, J. Okawauchi, K. Hiramatsu, and M. Harada, “Phosphorus sorption from aqueous solution using natural materials,” *Environ. Earth Sci.*, vol. 68, no. 3, pp. 859–863, Feb. 2013, doi: 10.1007/s12665-012-1789-6.

[136] I. Maamoun *et al.*, “Rapid and efficient chromium (VI) removal from aqueous solutions using nickel hydroxide nanoplates (nNiHs),” *J. Mol. Liq.*, vol. 358, p. 119216, Jul. 2022, doi: 10.1016/j.molliq.2022.119216.

[137] “Safety Data Sheet: Progesterone.” Tokyo Chemical Industry (India) Pvt. Ltd, May 13, 2023.

[138] L. V. M. da Rocha, P. S. R. C. da Silva, D. de H. S. Souza, and M. I. B. Tavares, “Molybdenum trioxide (MoO3): a scoping review of its properties, synthesis and applications: Trióxido de molibdênio (MoO3): uma revisão de escopo de suas propriedades, síntese e aplicações,” *Concilium*, vol. 24, no. 6, Art. no. 6, Apr. 2024, doi: 10.53660/CLM-3190-24F41.

[139] Y. Tian, L. Wang, T. Cheng, C. Chen, Y. Shi, and Q. Deng, “Application of MoO3 as an efficient catalyst for wet air oxidation treatment of pharmaceutical wastewater (Experimental and DFT study),” *Arch. Environ. Prot. 2021 Vol 47 No 2 47-60*, 2021, Accessed: Jul. 13, 2024. [Online]. Available: https://journals.pan.pl/dlibra/publication/137277/edition/119727

[140] W. Zhou, J. Deng, Z. Qin, R. Huang, Y. Wang, and S. Tong, “Construction of MoS2 nanoarrays and MoO3 nanobelts: Two efficient adsorbents for removal of Pb(II), Au(III) and Methylene Blue,” *J. Environ. Sci.*, vol. 111, pp. 38–50, Jan. 2022, doi: 10.1016/j.jes.2021.02.031.

[141] Congyi Zhang, Zhigang Pan, and Yaqiu Tao, “Synthesis and Catalytic Performance of Mo2C/MoS2 Composite Heterojunction Catalysts,” *Materials*, vol. 17, no. 10, May 2024, doi: https://doi.org/10.3390/ma17102355.

[142] N. Gaur, D. Dutta, A. Singh, R. Dubey, and D. V. Kamboj, “Recent advances in the elimination of persistent organic pollutants by photocatalysis,” *Front. Environ. Sci.*, vol. 10, Nov. 2022, doi: 10.3389/fenvs.2022.872514.

[143] “チオ尿素、ACS 試薬、≥ 99.0 NH2CSNH2.” Accessed: Jun. 14, 2024. [Online]. Available: http://www.sigmaaldrich.com/

[144] “12054-85-2・Ammonium Molybdate Tetrahydrate・019-03212・011-03211・013-03215[Detail Information] | [Common Chemicals & Lab Tools],” Laboratory Chemicals-FUJIFILM Wako Pure Chemical Corporation. Accessed: Jul. 14, 2024. [Online]. Available: https://labchem-wako.fujifilm.com/asia/product/detail/W01W0101-0321.html

[145] O. A. M. Falyouna, “Synthesis of Novel Iron-based Nanomaterials for the Removal of the Antibiotic Ciprofloxacin from Water,” *Kyushu Univ. Libr.*, doi: https://hdl.handle.net/2324/6787659.

[146] Clara Fernandes, Manasi Jathar, Bhakti Kubal Shweta Sawant, and Tanvi Warde, “Scale-Up of Nanoparticle Manufacturing Process | SpringerLink,” pp. 173–203, Jul. 2023.

[147] H. Huang, N. Liu, X. Wang, M. Zhong, and X. Huang, “Application of Hydrothermal and Solvothermal Method in Synthesis of MoS2,” *Rev. Chim.*, vol. 73, no. 4, pp. 26–35, Oct. 2022.

[148] I. Maamoun, R. Eljamal, and O. Eljamal, “Statistical optimization of nZVI chemical synthesis approach towards P and NO3− removal from aqueous solutions: Cost-effectiveness & parametric effects,” *Chemosphere*, vol. 312, p. 137176, Jan. 2023, doi: 10.1016/j.chemosphere.2022.137176.

[149] Y. Zhao, J. Xu, and X. Jiang, “DNA Cleavage by Chemically Exfoliated Molybdenum Disulfide Nanosheets,” *Environ. Sci. Technol.*, vol. 55, no. 6, pp. 4037–4044, Mar. 2021, doi: 10.1021/acs.est.1c00115.

[150] S. Takami, O. Eljamal, A. M. E. Khalil, R. Eljamal, and N. Matsunaga, “Development of Continuous System Based on Nanoscale Zero Valent Iron Particles for Phosphorus Removal,” *J. JSCE*, vol. 7, no. 1, pp. 30–42, 2019, doi: 10.2208/journalofjsce.7.1_30.

[151] Y. Fang, “Application of Molybdenum Disulfide Nanomaterials in Wastewater Treatment,” *Acad. J. Sci. Technol.*, vol. 7, no. 3, Art. no. 3, Oct. 2023, doi: 10.54097/ajst.v7i3.12722.

[152] Y. Liu *et al.*, “The peroxidase-like cleaning strategy for organic fouling of water treatment membranes based on MoS2 functional layers,” *J. Water Process Eng.*, vol. 54, p. 103955, Aug. 2023, doi: 10.1016/j.jwpe.2023.103955.

[153] S. Sarkar and S. Ahuja, “Chapter 2 - Importance of nanomaterials in water purification,” in *Separation Science and Technology*, vol. 15, S. Ahuja, Ed., in Separations of Water Pollutants with Nanotechnology, vol. 15. , Academic Press, 2022, pp. 13–36. doi: 10.1016/B978-0-323-90763-7.00002-0.

Supplementary Data

Supplementary Table 1: Preliminary tests using NZVI and NZVI-based nanoparticles for the removal of Progesterone from water.

Adsorbent	Dose (mg L^{-1})	Treatment time	
		1hr	2hr
NZVI + Mg	0.5	19.72	15.41
	1	19.49	6.35
	1.5	16.55	13.15
Bare NZVI	0.1	45.79	13.37
	0.3	37.63	37.4
	0.5	46.01	67.32
	0.7	26.75	13.6
	1	43.75	52.36
	1.5	0.23	35.59
	2	100	39.44
Oxalate + NZVI (0.5mM)	0.5	37.66	34.32
Oxalate + EDT (0.5mM)	0.1	53.15	42.06
	0.5	37.14	13.73
Oxalate (0.3 mM)	0.1	46.74	45.79
	0.2	11.41	37.39
	0.3	5.23	28.83
	0.4	18.22	32.64
	0.5	21.07	12.67
Ascorbic Acid (0.5mM)	0.1	30.06	34.54
	0.2	36.50	24.54
	0.3	43.23	26.85
	0.4	45.23	24.55
	0.5	34.21	32.87

Hydrogen Peroxide (0.5mM)	0.1	56.33	46.75
	0.2	49.03	43.23
	0.3	46.12	33.27
	0.4	32.15	32.12
	0.5	24.35	21.34
Optimizing Bare NZVI	0.1	31.28	3.23
	0.3	8.16	29.41
	0.5	42.84	35.53
	0.7	58.31	21.25
	0.9	45.73	35.35
75% Dilution	0.1	35.22	27.17
	0.3	31.2	33.88
	0.5	-51.33	29.19
	0.7	-66.09	30.53
	1	60.05	-100.65
50% Dilution	0.1	29.19	26.5
	0.3	29.19	33.55
	0.5	-52	34.22
	0.7	-61.39	30.53
	1	-54.37	-106.68

Supplementary Table 2: Long term progesterone removal experiment using NZVI nanoparticles from 5 – 36 hours.

time (hrs)	NZVI Dose (mg L^{-1})				
	0.1	**0.3**	**0.5**	**0.7**	**0.9**
0	0.00	0.00	0.00	0.00	0.00
5	17.54	9.59	-89.96	-73.85	-50.80
7	6.73	23.46	-100.78	-66.30	-181.77
9	19.58	22.44	-142.60	-101.59	-111.59

11	34.27	34.68	8.77	-128.93	-6.73
13	22.44	46.92	23.87	16.12	21.22
15	28.76	33.25	19.99	19.99	14.08
17	51.82	42.02	23.05	38.76	24.48
19	47.53	56.51	31.82	25.09	33.86
21	41.41	70.79	33.05	33.66	27.74
36	76.30	80.38	31.82	89.35	20.20

Supplementary Table 3: Long term progesterone removal experiment using NZVI nanoparticles from 1 – 24 hours.

Time (hrs)	NZVI Dose (mg L^{-1})				
	0.1	**0.3**	**0.5**	**0.7**	**0.9**
0	0.00	0.00	0.00	0.00	0.00
1	46.42	-5.55	-15.37	-25.19	-27.41
2	40.72	20.60	-14.89	-35.01	-24.87
3	45.94	38.18	-13.78	-36.76	-40.56
4	35.17	42.30	42.78	-30.10	-39.13
5	40.08	38.34	43.57	-29.63	-75.73
6	35.49	41.83	41.67	39.13	-66.54
7	37.39	43.09	39.61	37.07	38.34
8	23.13	36.60	41.03	31.37	42.62
9	32.95	35.65	37.55	34.38	34.38
10	33.43	41.35	89.03	35.65	35.81
24	31.84	93.32	93.32	79.06	68.44